Monthly Notices of the ROYAL ASTRONOMICAL SOCIETY

MNRAS **496,** 5262–5281 (2020) doi:10.1093/mnras/staa1867
Advance Access publication 2020 July 2

Centroid frequency ratios of simultaneous low-frequency QPOs in black hole low-mass X-ray binaries

Marieke van Doesburgh ★ and Michiel van der Klis
Anton Pannekoek Instituut, 1098 XH Amsterdam, the Netherlands

Accepted 2020 June 17. Received 2020 June 17; in original form 2020 March 21

ABSTRACT

We measure the centroid frequency ratios of simultaneous quasi-periodic oscillations (QPOs) that occur at low frequency (0.1–30 Hz) in a selection of accreting black hole (BH) low-mass X-ray binaries. We use all data in the RXTE archive on GX 339–4, GRO J1655–40, 4U 1630–47, XTE J1550–564, and H 1743–322. We select the power spectra that show at least two simultaneous QPOs, and empirically divide them into four main categories, whose occurrence correlates systematically to X-ray spectral state. In the hard/hard-intermediate state, all sources show sets of QPO peaks with near-harmonic frequency relations, which we measure as precisely as possible using an improved analysis method. We find small but significant offsets from purely harmonic frequency relations that in most cases can be explained by the fit function not describing the QPOs accurately; for some QPO pairs, however, the 'sub-harmonic' is at a higher frequency than expected. In the intermediate and ultraluminous states, in all sources we find non-harmonic QPO pairs, some previously reported. We distinguish several different types of non-harmonic QPO pairs that occur across sources. We discuss these findings in the framework of classification schemes and models proposed for black hole low-frequency QPOs. We conclude that the phenomenology of the frequency ratios indicates that in addition to the physical mechanism (possibly precession) explaining the common harmonically related sets of (Type B and C) QPO peaks, at least one additional mechanism is required to explain the occurrence of pairs of QPOs in other states that are not only not harmonically related, but also stand out by the absence of harmonics to either of them.

Key words: accretion, accretion discs – binaries: close – X-rays: binaries.

1 INTRODUCTION

Low frequency (LF) quasi-periodic oscillations (QPOs) are often observed in the X-ray emission of accreting black hole (BH) low-mass X-ray binaries (LMXBs). They appear in the ∼0.1–30 Hz frequency range of the Fourier power spectrum of the light curve as narrow peaks, with $Q \gtrsim 5$ (quality factor $Q = \frac{\nu}{\mathrm{FWHM}}$). Their frequencies, fractional rms amplitudes, and the presence of detectable (sub-)harmonics are correlated to the energy spectral state of the source which evolves during outburst.

These spectral states are generally subdivided into three main categories based on the luminosity and relative number of photon counts in soft and hard energy bands: the hard state, the intermediate states, and the soft state (e.g. Belloni & Motta 2016, in this classification the *very high state* as defined by Miyamoto et al. 1991 is part of the intermediate states). Additionally, some sources show excursions to an ultraluminous state (also known as the anomalous state) at high luminosities during outburst (see Ingram & Motta 2020 for a recent review).

LF QPOs come in a variety of types and sub-types that occur throughout one or several of these spectral states. Those seen in XTE J1550–564 were the first to be categorized into three main types (Wijnands, Homan & van der Klis 1999; Remillard et al. 2002), Type A, B, and C; some of these have since been reclassified based on comparisons with other sources (Casella, Belloni & Stella 2005). The majority of QPOs are of Type C: a strong sharp (up to ∼20 per cent rms, $Q \gtrsim 8$) QPO atop strong band-limited noise often accompanied by (sub-)harmonics[1] at one half, twice and three times the fundamental frequency and whose frequencies increase as the source state evolves from hard to soft. Type B QPOs (with up to ∼5 per cent rms and $Q \gtrsim 6$) are also seen with (sub-)harmonics at integer frequency ratios with the fundamental, but with markedly less noise than Type C QPOs and mainly in the intermediate states. Type B and C QPOs overlap in frequency, although for Type C QPO the range of frequencies is much larger (up to ∼30 Hz) than for Type B (∼10 Hz). Type A QPOs are rare and typically appear with frequencies of ∼7 Hz without harmonics in the soft/soft-intermediate state (they are broader than Type B and C QPOs: $Q \lesssim 3$).

The majority of simultaneous LF QPOs reported have approximately integer frequency ratios. Examples of simultaneous QPOs previously reported in the literature to have non-integer frequency ratios include, first, double QPOs in H 1743–322 with frequencies that differed by a factor 1.931 ± 0.014 (Homan et al. 2005b).

★ E-mail: m.j.vandoesburgh@uva.nl

[1] We use the term 'QPO' to refer to one single peak in the power spectrum, and, aware of the difficulty physical models have to explain the occurrence of true sub-harmonics, we use the term 'sub-harmonic' in this work as a label only.

Secondly, a QPO with a wing a factor 1.5–1.8 higher reported in XTE J1550–564 (Wijnands et al. 1999). These QPOs in H 1743–322 and XTE J1550–564 have been classified as belonging to a subcategory of Type B QPOs (Casella et al. 2005). Thirdly, there are many accounts of two simultaneous QPOs seen in the ultraluminous state with frequencies that are more than a factor 2 apart, see Choudhury, Bhatt & Bhattacharyya (2015) for 4U 1630–47, Homan et al. (2005a) and Motta et al. (2012) for GRO J1655–40, Motta et al. (2014b) for XTE J1550–564 and Li et al. (2014) for GRO J1655–40, H 1743–322 and XTE J1550–564. These QPOs in GRO J1655–40 were classified as a Type B QPO occurring simultaneously with a Type C QPO (Motta et al. 2012), and argued to support the view that Type B and Type C QPOs are different and originate from two distinct physical mechanisms. And lastly, a QPO that jumps between two frequencies, lower within dips in the light curve, and higher outside the dips and that is seen together with a stable QPO at a frequency a factor ∼1.5 or ∼3.5 higher in 4U 1630–47 (so that altogether three QPO peaks appear in the average power spectrum, Dieters et al. 2000).

The harmonic content of X-ray variability is a key ingredient of many LF-QPO models. Two main categories of models exist for the physical mechanism producing the QPOs: those that invoke precession of (parts of) the accretion flow due to frame dragging (e.g. Stella & Vietri 1998; Schnittman, Homan & Miller 2006; Ingram, Done & Fragile 2009), and those that use intrinsic oscillations in the accretion flow (e.g. Tagger & Pellat 1999; Wagoner, Silbergleit & Ortega-Rodríguez 2001).

The geometry of the precessing hot inner flow in the model by Ingram et al. (2009) can account for multiple QPOs at integer frequency ratios. Their relative strengths may differ between multiple wavebands depending on the angles between the system and the observer, and between the inner flow, the disc, and the jet. The disc can be illuminated alternatingly by the top and bottom part of the inner flow; the strongest X-ray QPO is then expected at twice the precession frequency. The infrared QPO reported by Kalamkar et al. (2016) at a factor two lower frequency than a simultaneous X-ray QPO can be explained within this framework: in the infrared the jet contributes most to the emission, so a stronger QPO occurs at the precession frequency.

The precession models are supported by observations of the fractional rms dependence of certain QPOs on source inclination (Schnittman et al. 2006; Motta et al. 2015) and modulation of the iron line energy on the QPO period (Ingram et al. 2016).

Examples of models that use intrinsic flow oscillations to explain the QPOs include the transition layer model proposed by Titarchuk, Lapidus & Muslimov (1998). This model can account for deviations from integer QPO frequency ratios due to damping and shifts of resonance frequencies (Titarchuk 2002). Within the framework of the disco-seismic oscillation models (e.g. Wagoner et al. 2001), internal pressure, and corrugation modes with non-integer frequency ratios could occur simultaneously. The accretion ejection instability model (e.g. Tagger & Pellat 1999; Varnière, Tagger & Rodriguez 2012) also predicts frequency ratios close to, but not exactly at, integers. Finally, of course, any quasi-periodicity that is non-sinusoidal will show harmonics in a Fourier analysis, which can combine or blend with QPO peaks arising in other ways.

Clearly, much can be gained from an overview of simultaneous QPO frequency ratios, where integers suggest a common physical origin that might be as simple as a non-sinusoidal modulation, but could also indicate different co-precessing geometries or harmonically related modes, near-integers might point at specific models such as those mentioned above, and non-integers might indicate the coincidence of otherwise unrelated oscillations. Here, we provide such an overview of different types of simultaneous QPOs analysed in a systematic way for a selection of BH systems and provide a link to the A/B/C classification. Using an optimized method, we accurately measure the relations between these QPO frequencies. We discuss our results in the context of proper phenomenological classification and the models mentioned.

2 METHODS AND OBSERVATIONS

We use all available RXTE data on black holes (BHs) GX 339–4, GRO J1655–40, 4U 1630–47, H 1743–322, and XTE J1550–564 which have many reported simultaneous LF QPOs (e.g. Motta et al. 2015; de Ruiter et al. 2019). In total we use 3631 observations of typically ∼3 ks in length. Per observation we extract the Crab-normalized hard colour (HC, the ratio of counts in the 16.0–20.0 and 2.0–6.0 keV energy bands) and intensity (in the 2–20 keV band) using Standard 2 data in good time intervals determined by applying customary filtering (e.g. van Straaten et al. 2002). We use Event, Binned, Good Xenon, or Single Bit modes with time resolution of 1/8192 s or better (in a few cases we use the best available 1/4096 s resolution) to calculate FFTs using 16 s (or 128 s for observations in the low hard state) data segments including all available energy channels. We average the Leahy-normalized power spectra over the total length of an observation. Then, before fitting, we subtract a counting noise model spectrum that takes dead-time effects into account (Zhang et al. 1995) as described by Klein Wolt (2004), shifting the noise level by typically 0.5 per cent to match the power in a high-frequency range (0.75–1 × the Nyquist frequency) where no source signal is expected. We normalize the power spectra such that the square root of the integrated power (IP) in the spectrum equals the fractional root mean square (rms) of the variability in the signal, as described in van der Klis (1989) (for more information on timing analysis in general we refer the reader to this work).

We carefully examined each power spectrum and selected only those that clearly exhibited multiple QPOs. We also included power spectra showing, in addition to a QPO with $\nu \gtrsim 10$ Hz, a peaked noise feature at approximately half the QPO frequency in the intermediate states as in these cases this feature likely results from averaging over a rapidly moving QPO peak (see Dieters et al. 2000). We focus on the 0.1–30 Hz frequency range, excluding any mHz and high-frequency QPO phenomena. We use a multi-Lorentzian model (with as parameters centroid frequency ν_i, where i identifies the QPO, full width at half maximum (FWHM) and IP from 0 to infinity) to fit the power spectra. In addition to the QPOs and peaked noise components as described, we find that one or two broad noise components, producing shoulders at low (<10 Hz) and high (>50 Hz) frequency are required for an acceptable fit. In some cases, we add an extra component with low fractional rms to account for an asymmetric QPO wing towards higher frequency. The centroid frequency of the QPO is barely affected by this (it is typically 1 per cent lower when the component is added, in Fig. A5, an example of this kind of power spectrum is plotted). We neither discuss these power spectral features in much further detail, nor do we use them to categorize power spectra.

For observations longer than ∼6 ks, we check whether the average flux varies by more than 10 per cent during the observation. If so, we divide the data into several shorter time intervals of typically ∼2 ks such that the effects of QPO frequency drift are limited but the QPOs can still be detected at ∼3σ or more. We use the method described in van Doesburgh & van der Klis (2017) to scan $\Delta\chi^2$ maps for all QPO centroid frequency pairs. We use these maps as input

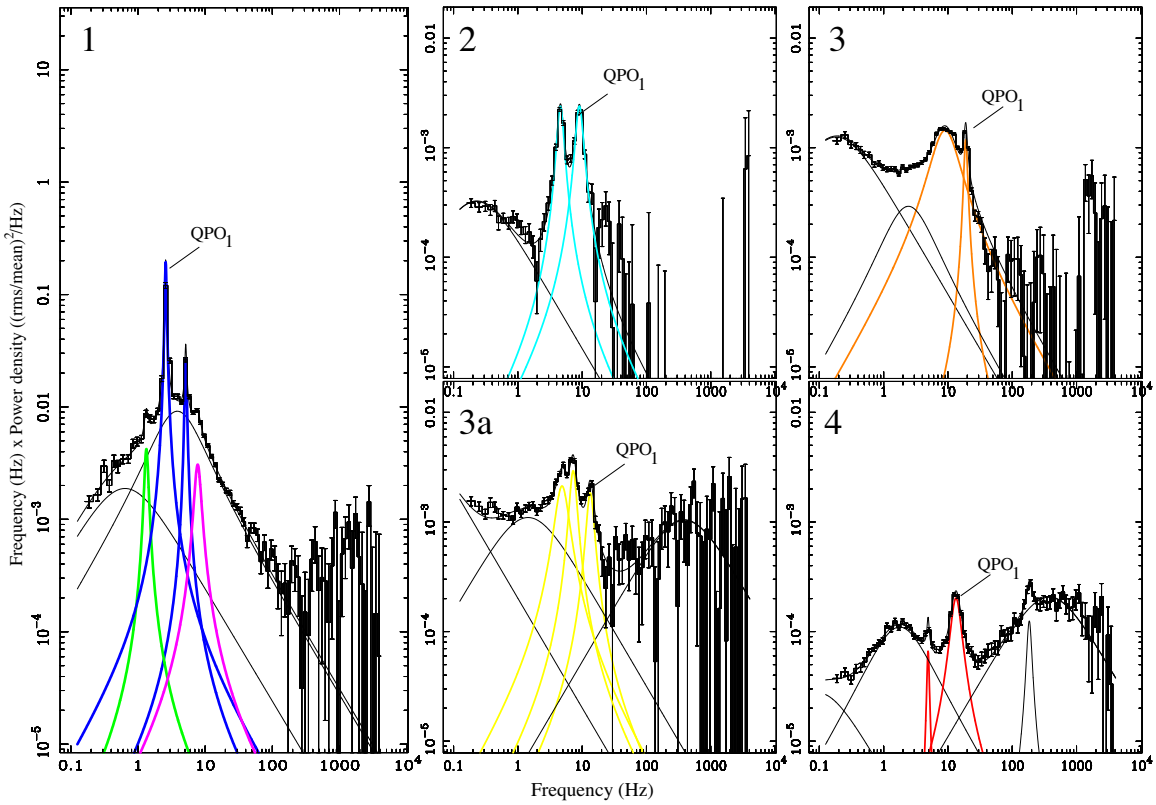

Figure 1. Representative power spectra with our choice for benchmark QPO_1 indicated for each category in our sample. The observations used are: 30188-06-10-00 (Group 1, XTE J1550–564), 80146-01-62-00 (Group 2, H 1743–322), 91702-01-54-00 (Group 3, GRO J1655–40), 30178-01-10-00 (Group 3a, 4U 1630–47), and 30191-01-02-00 (Group 4, XTE J1550–564). The vertical scale and lower bound are the same in each frame to exhibit differences in feature strengths between groups.

to a simple proportionality fit[2] $\nu_n = a \cdot \nu_1$, where ν_1 is the centroid frequency of a QPO we designate QPO_1, and ν_n that of QPO_n, which may or may not be precisely harmonically related to ν_1, and give accurate values and errors for the best-fitting proportionality constants (a) of the frequency–frequency relations if such a fit is appropriate.

3 RESULTS

When focusing, as we do in this work, exclusively on the multiple-QPO power spectra of the five sources in our sample, we find that for these power spectra a subdivision in four general groups imposes itself. This grouping is of course phenomenological and primarily motivated by the aim of studying the frequency–frequency relations in a tractable way. It does lead to groups of power spectra across sources, however, that show very similar relations between the QPO frequencies, and to an extent also between the other characteristics of the QPOs. In Fig. 1, we show one representative power spectrum for each group. For purposes of plotting frequency–frequency relations, we assign a benchmark QPO, 'QPO_1', as indicated in Fig. 1. We stress this does not prejudge which QPOs are the same physical phenomenon or which are the 'fundamental' QPO. We discuss the different groups of power spectra seen in each source in further detail in Appendix A. We note that not all sources show each type of power spectrum; see Table 1 for the number of averaged power spectra in each group and the total number of observations per source. The relative number of averaged power spectra per group differs per source. For 4U 1630–47 for instance, most observations fall in Group 4, while for GX 339–4 and XTE J1550–564 Group 1 is dominant. The colour coding for the QPOs in each group as shown in Fig. 1 applies to all figures in this work. The characteristics of each group can be summarized as follows:

(i) Group 1, encountered in the hard/hard-intermediate states, has power spectra featuring a QPO with strong ∼5–10 per cent fractional

[2]As explained in van Doesburgh & van der Klis (2017), in cases where a secondary minimum is found that does not probe the frequency of the power spectral feature of interest, we extrapolate the map using an elliptical paraboloid extrapolation method. In this work, we extrapolated fewer than 6 per cent of all maps.

Table 1. The number of observations used in this work with more than one QPO, the number of observations with single QPOs (where harmonics are not significantly detected or no harmonics are present, see main text for references), and the total number of available observations in the RXTE archive per source. We give the number of averaged power spectra (pds) used per group, which can be larger than the number of observations as we breakup long ($\gtrsim$6 ks) observations that show gradual flux variations into shorter time segments.

Source	#Obs >1 QPO	#Obs 1 QPO	#Obs Tot.	#pds Gr. 1	#pds Gr. 2	#pds Gr. 3	#pds Gr. 3a	#pds Gr. 4
GX 339–4	52	78	1019	59	3	0	0	0
GRO J1655–40	53	35	585	16	3	32	10	2
4U 1630–47	42	19	1096	2	9	11	10	19
XTE J1550–564	70	24	391	63	6	1	0	1
H 174–322	99	100	540	51	41	12	0	2

rms, high Q factor (5–15), and centroid frequency ν_1 below 15 Hz (QPO_1, plotted in *blue*), accompanied by one or more of three weaker (in most cases by at least a factor of 2 in rms) (sub-)harmonics at, or near, $\nu_{\frac{1}{2}} \approx 0.5\nu_1$ ($QPO_{\frac{1}{2}}$, plotted in *green*), $\nu_2 \approx 2\nu_1$ (QPO_2, also plotted in *blue*), or $\nu_3 \approx 3\nu_1$ (QPO_3, plotted in *magenta*). These power spectra can have high (Type C) or low (Type B) noise levels beneath the QPOs.

(ii) Group 2, in the soft/soft-intermediate states (plotted in *cyan*) shows double QPOs with relative QPO strengths that are similar, varying a bit between observations but typically differing by less than a factor of 2 in rms. These additionally stand out from Group 1 QPOs in terms of fractional rms (at least a factor 2 lower), and by non-integer frequency ratios ($\nu_2 < 2\nu_1$). QPOs mentioned in the introduction reported by Wijnands et al. (1999) and Homan et al. (2005b) for XTE J1550–564 and H 1743–322, respectively, fit this category. These QPOs were classified as 'cathedral' QPOs, a subtype of Type B QPOs (Casella et al. 2005). We arbitrarily designate the QPO at highest frequency to be QPO_1, and the one at lower frequency as $QPO_{\frac{1}{2}}$.

(iii) Group 3, in the intermediate states (plotted in *orange*): power spectra with a QPO (with centroid frequency typically >10 Hz, and $Q \sim 5$) and a peaked noise feature (with $Q \sim 0.75$–2) at approximately half the QPO frequency. Examples in the literature include power spectra reported for GRO J1655–40 (designated 'Type 2' in Motta et al. 2012) and 4U 1630–47 (Dieters et al. 2000; Trudolyubov, Borozdin & Priedhorsky 2001). In these cases, we identify the peaked noise as $QPO_{\frac{1}{2}}$ and the QPO above 10 Hz as QPO_1. Dieters et al. (2000) show power spectra of this type in their analysis of the 1998 outburst of 4U 1630–47 with, instead of a peaked noise feature, one QPO that due to rapid frequency variations appears as two QPOs in the power spectrum. As we mentioned earlier, the QPO shows jumps in frequency which are related to dips in the light curve. Such power spectra are not only encountered in 4U 1630–47 but also in GRO J1655–40. We report them as Group 3a (plotted in *yellow*) keeping in mind that there might be only one underlying QPO with a variable frequency. It is possible that in Group 3, similarly, the peaked noise also originates from a QPO with rapidly varying frequency. In the literature, in most cases the >10 Hz QPO is classified as Type C (e.g. Motta et al. 2015).

(iv) Group 4, in the ultraluminous state (plotted in *red*): double QPOs with fractional rms ∼1 per cent and not at an integer frequency ratio. As mentioned in the introduction, these QPOs have been reported as a simultaneous Type B and Type C QPO. We define the QPO at highest frequency to be QPO_1, and the one at lower frequency as $QPO_{\frac{1}{2}}$.

By applying this identification scheme the frequency of QPO_1 increases smoothly towards softer states in the hardness-intensity diagram (HID) in most sources, preventing clutter in the frequency–frequency plots. Our naming scheme for the QPOs (e.g. $QPO_{\frac{1}{2}}$, QPO_1, QPO_2, QPO_3) draws from approximate frequencies, which in Group 1 approximately matches the measured frequency ratios. In Groups 2–4, we only use $QPO_{\frac{1}{2}}$ and QPO_1; $QPO_{\frac{1}{2}}$ corresponds to two different peaks in Group 3a.

In Figs 2(a), 3(a), 4(a), 5(a), and 6(a), we plot centroid frequencies of the relevant peaked noise and QPO features fitted in the same power spectrum versus ν_1 (the centroid frequency of QPO_1). The error bars indicate the extremes of the 2-parameter 99 per cent confidence contour ($\Delta\chi^2 = 9.21$) of the best-fitting centroid frequencies for a given frequency pair. Most of these QPOs have been previously reported to belong to class A, B, and/or C, and we indicate these classifications with different plot symbols (*squares*, *stars*, and

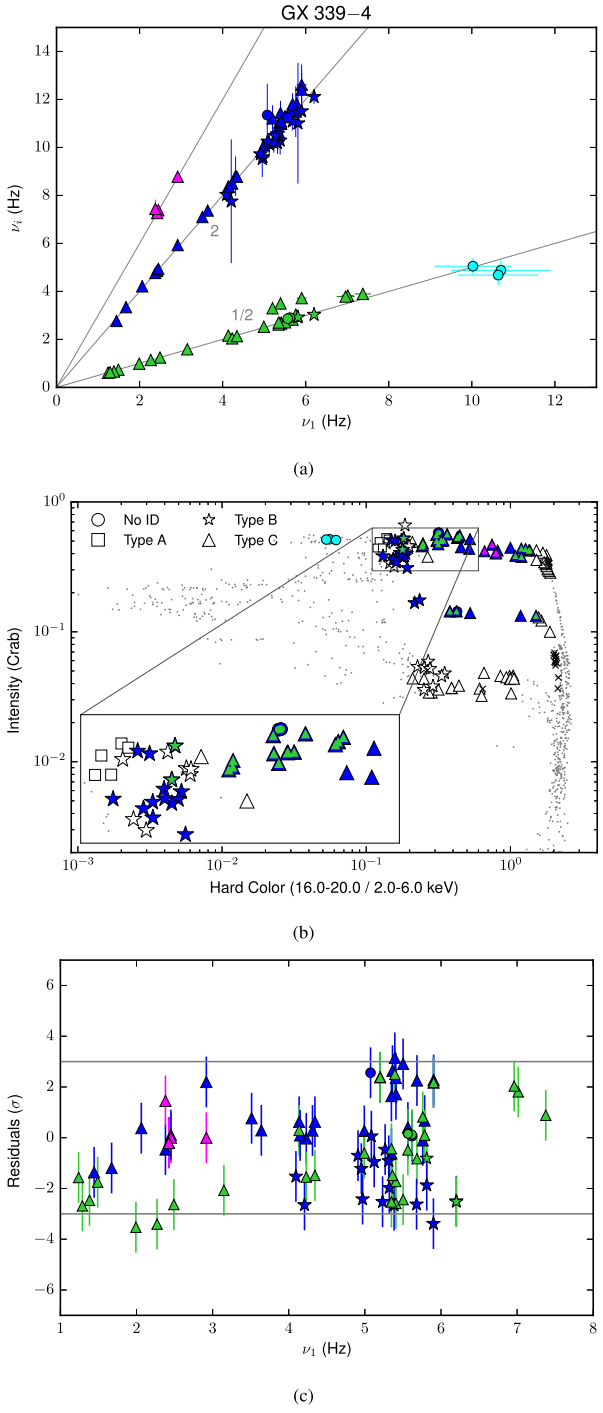

Figure 2. (a) QPO frequencies for GX 339–4. Integer frequency ratios are indicated with *grey* lines and numbers. Error bars indicate the size of the 99 per cent 2-parameter confidence contour and can be smaller than the symbols. QPOs identified as Type A, B, or C in the literature (see the main text for references) are indicated with *squares*, *stars,* and *triangles*, respectively. QPOs not previously classified in this way are indicated with *circles*. (b) Hard colour versus intensity for all observations of GX 339–4 in the RXTE archive in *grey*. The observations with multiple QPOs are plotted here using the same colours and symbols as in panel (a). Single QPOs not used in this work, but reported in previous works, are indicated with *open* symbols. Observations with single QPOs not reported in the literature are indicated with *crosses*; most of these occur at HC $\gtrsim$ 1. (c) Residuals from the best-fitting proportionality fit to frequencies from power spectra in Group 1 shown in panel (a). Colours and symbols are the same as in panel (a).

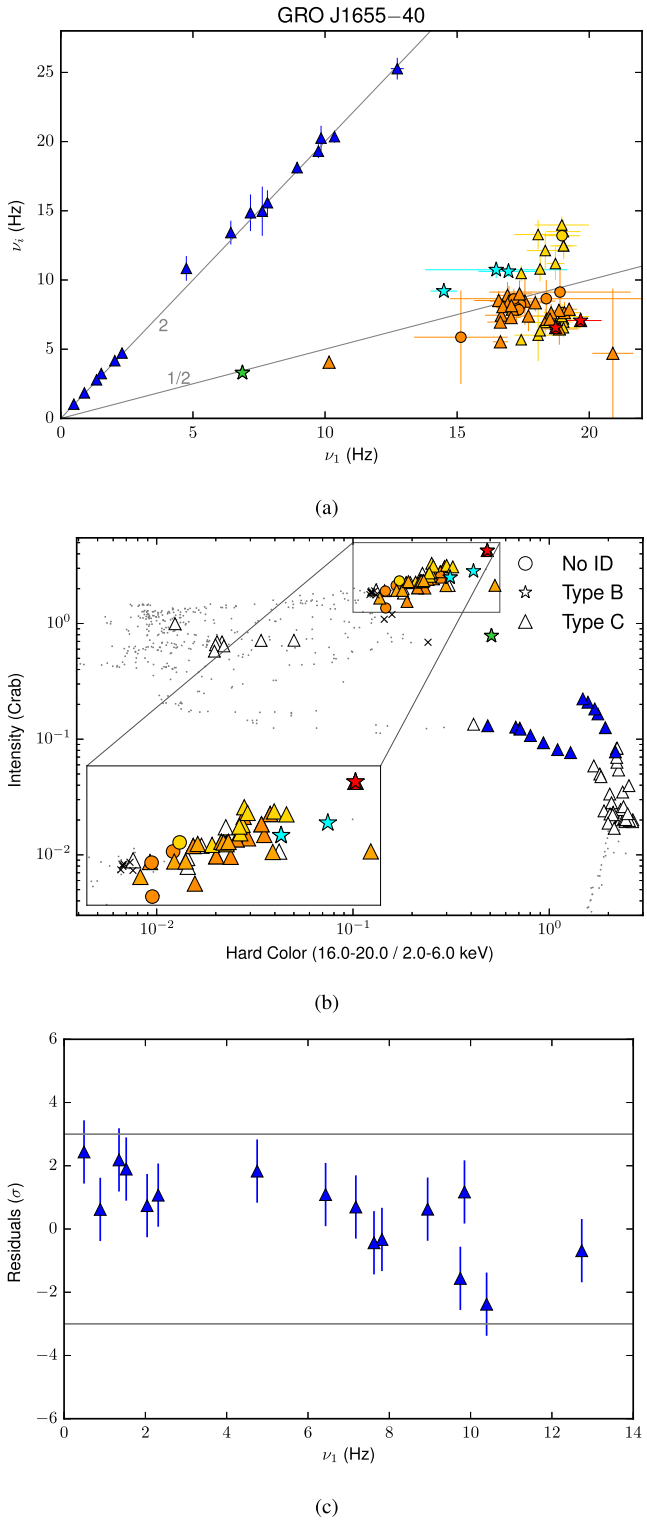

Figure 3. As in Fig. 2, but for GRO J1655–40. Power spectra with reported simultaneous Type B and C QPOs by Motta et al. (2015) are indicated with overlapping *red stars* and *triangles*.

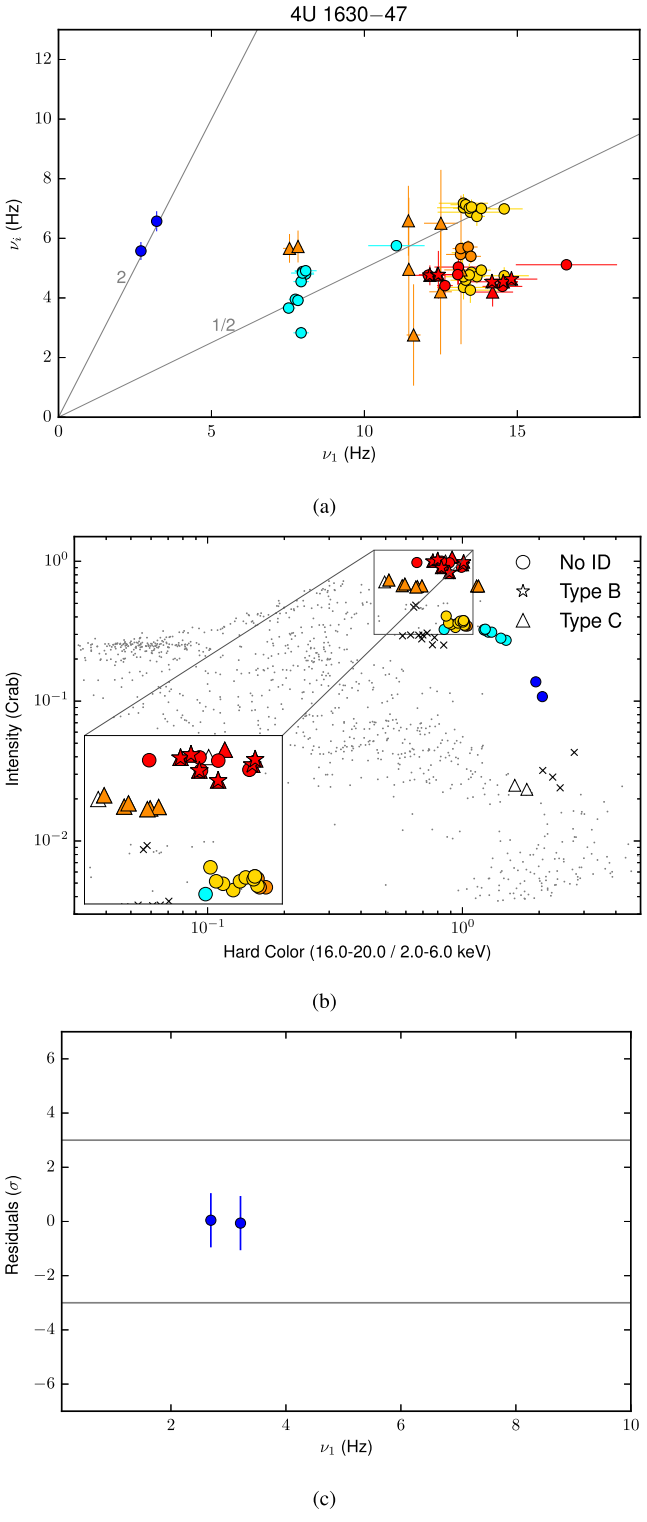

Figure 4. As in Fig. 2, but for 4U 1630–47. Power spectra with reported simultaneous Type B and C QPOs by Motta et al. (2015) are indicated with overlapping *red stars* and *triangles*.

triangles, respectively). For this, we use the following references: Motta et al. (2015) for all sources, and additionally: Motta et al. (2014b) and Remillard et al. (2002) for XTE J1550–564, Motta et al. (2011) for GX 339–4, and Gao et al. (2017) for H 1743–322, XTE J1550–564 and GX 339–4. If a QPO type was not reported in these previous works, we use a circle. If different classifications of the same QPO exist, we use the one reported in the most recent work, see the Appendix for details.

In Figs 2(b), 3(b), 4(b), 5(b), and 6(b), we plot the HIDs of our sources using all observations in the RXTE archive in *grey*, and the

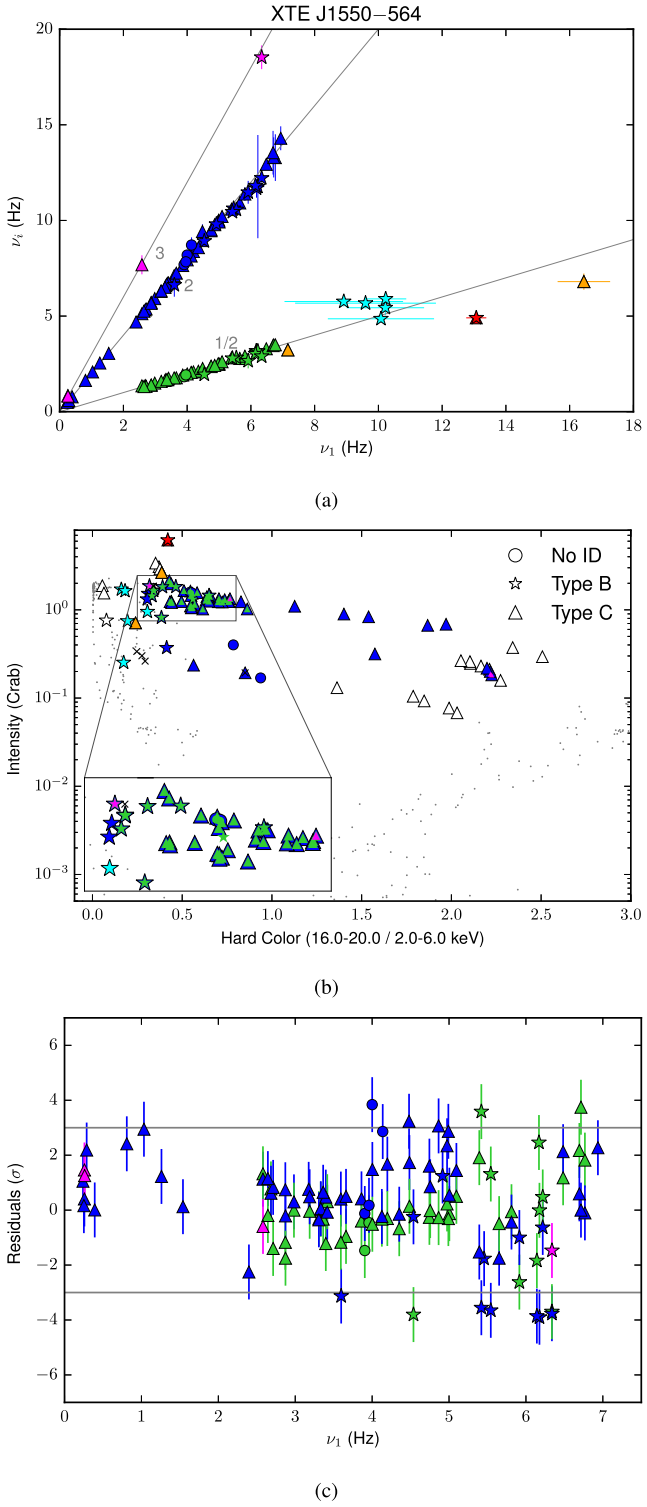

Figure 5. As in Fig. 2, but for XTE J1550. The *red* power spectrum contains a simultaneous Type B and C QPO, as reported by Motta et al. (2015).

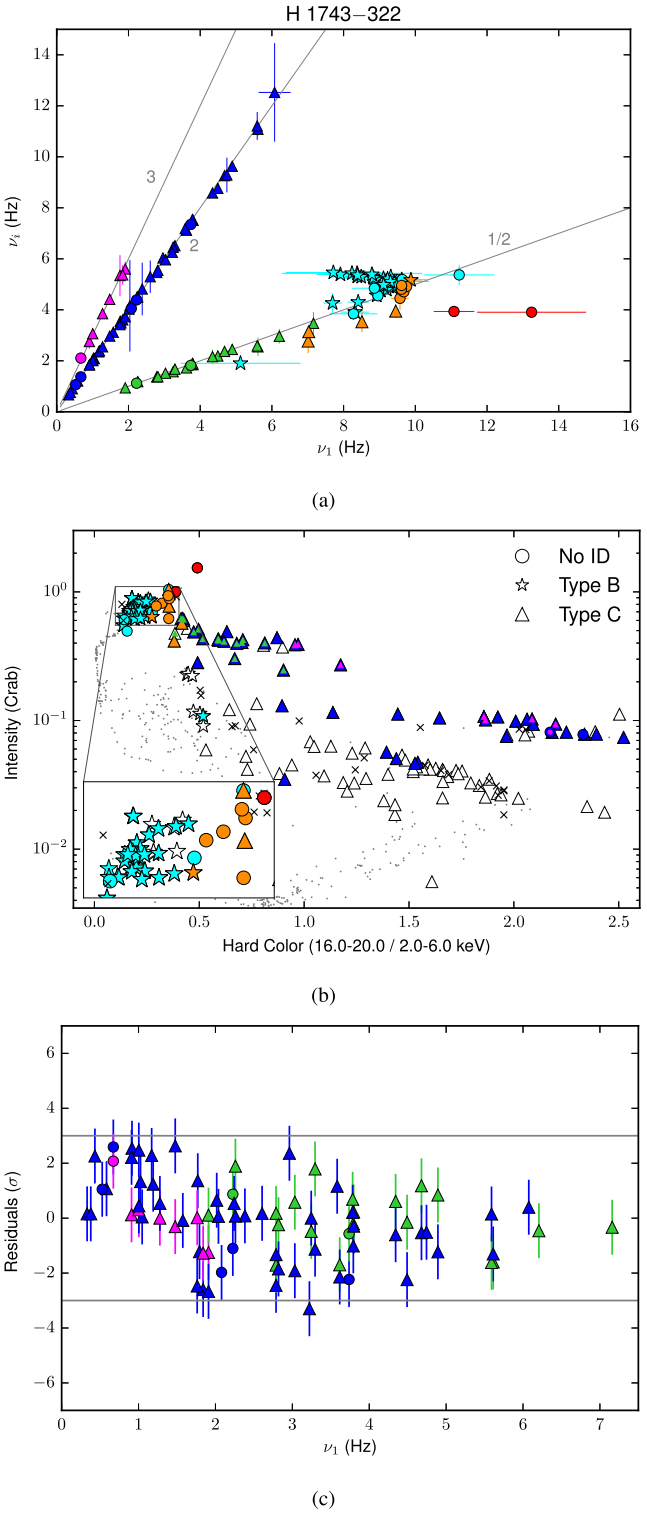

Figure 6. As in Fig. 2, but for H 1743–322.

observations containing the QPOs reported in Table 2. The *open* symbols refer to single QPOs that were not included in this work for lack of other QPOs in the same power spectrum, but were reported in Remillard et al. (2002), Motta et al. (2011, 2014b, 2015), or Gao et al. (2017). We indicate other observations where we find a single QPO with *crosses* in the HIDs. Towards lower intensity, where the majority of single QPOs occur in the HID, the QPOs other than QPO_1 likely become undetectable due to decreasing signal-to-noise ratio. It is therefore to be expected that these QPOs are not intrinsically different from the multiple QPOs we report in this work, and that they would not significantly alter our grouping scheme if included in the analysis.

Table 2. Shortened table with Lorentzian fit parameters (QPO centroid frequencies ν_i, FWHM, IP) for each averaged power spectrum, sorted by source and group. The QPO significance is estimated from the negative error on the IP. Errors use $\Delta\chi^2 = 1$. In the last column, we quote previously reported Type A/B/C classifications, see main text for the references. The full table can be found at https://github.com/mariekevandoesburgh/harmonics.

Obs. ID	Start times	$QPO_{\frac{1}{2}}$				QPO_1				QPO_2				QPO_3				
	1st, last	ν_0 (Hz)	FWHM (Hz)	IP $\times 10^{-3}$	Sig. (σ)	ν_0 (Hz)	FWHM (Hz)	IP $\times 10^{-3}$	Sig. (σ)	ν_0 (Hz)	FWHM (Hz)	IP $\times 10^{-3}$	Sig. (σ)	ν_0 (Hz)	FWHM (Hz)	IP $\times 10^{-3}$	Sig. (σ)	Type
GX 339–4 Group 1																		
60705-01-69-01	*all*	–	–	–	–	1.44 ± 0.02	0.20 ± 0.07	2.32 ± 0.66	3.9	2.77 ± 0.02	0.08 ± 0.07	0.52 ± 0.20	2.8	–	–	–	–	C
60705-01-70-00	*all*	–	–	–	–	4.31 ± 0.02	0.27 ± 0.06	2.09 ± 0.34	6.2	8.80 ± 0.21	1.39 ± 0.89	1.28 ± 0.61	2.7	–	–	–	–	C
70109-04-01-00-1	0,2833	2.67 ± 0.04	0.75 ± 0.14	0.98 ± 0.19	5.4	5.36 ± 0.01	0.61 ± 0.04	4.16 ± 0.16	25.6	11.04 ± 0.08	1.78 ± 0.23	0.64 ± 0.08	8.7	–	–	–	–	C
70109-04-01-00-2	5696,8064	2.83 ± 0.04	0.47 ± 0.10	0.64 ± 0.13	5.2	5.57 ± 0.01	1.08 ± 0.06	4.95 ± 0.19	26.5	11.27 ± 0.08	2.45 ± 0.34	0.94 ± 0.11	9.3	–	–	–	–	C
70109-04-01-01-1	0,3519	2.62 ± 0.03	0.79 ± 0.15	1.24 ± 0.25	6.0	5.35 ± 0.01	0.65 ± 0.03	4.17 ± 0.15	29.8	10.88 ± 0.05	1.63 ± 0.19	0.72 ± 0.07	10.3	–	–	–	–	C
70109-04-01-01-2	5674,14907	2.71 ± 0.03	0.77 ± 0.12	0.98 ± 0.16	7.3	5.50 ± 0.01	0.68 ± 0.03	3.85 ± 0.11	38.2	11.30 ± 0.06	2.09 ± 0.20	0.74 ± 0.06	12.5	–	–	–	–	C
70109-04-01-01-3	17066,20614	2.69 ± 0.04	0.76 ± 0.13	1.15 ± 0.21	6.2	5.41 ± 0.01	0.58 ± 0.03	3.82 ± 0.14	28.5	11.08 ± 0.08	1.79 ± 0.28	0.72 ± 0.09	8.9	–	–	–	–	C
70109-04-01-01-4	22762,26314	2.66 ± 0.03	0.73 ± 0.13	1.03 ± 0.19	5.9	5.41 ± 0.01	0.67 ± 0.03	3.99 ± 0.14	27.6	10.99 ± 0.04	1.30 ± 0.14	0.64 ± 0.06	11.4	–	–	–	–	C
70109-04-01-02	*all*	2.70 ± 0.05	0.52 ± 0.14	0.83 ± 0.22	4.4	5.35 ± 0.02	0.91 ± 0.07	5.13 ± 0.28	20.7	10.64 ± 0.09	1.92 ± 0.43	1.08 ± 0.17	7.2	–	–	–	–	C
70110-01-10-00	*all*	–	–	–	–	2.06 ± 0.01	0.20 ± 0.03	3.75 ± 0.35	10.8	4.21 ± 0.06	0.41 ± 0.10	0.80 ± 0.16	5.0	–	–	–	–	C
70110-01-11-00	*all*	2.98 ± 0.08	0.96 ± 0.30	1.12 ± 0.43	3.2	5.79 ± 0.02	0.76 ± 0.09	3.78 ± 0.29	14.3	11.80 ± 0.15	1.80 ± 0.48	0.50 ± 0.11	4.8	–	–	–	–	C
90110-02-01-00	0,3360	3.50 ± 0.08	1.32 ± 0.39	1.78 ± 0.74	2.9	5.39 ± 0.02	0.49 ± 0.08	1.53 ± 0.19	8.3	11.44 ± 0.15	1.75 ± 0.47	0.75 ± 0.17	4.8	–	–	–	–	C
90110-02-01-00-2	5602,9030	3.55 ± 0.10	2.03 ± 0.46	3.48 ± 1.34	2.7	5.90 ± 0.04	0.64 ± 0.11	1.23 ± 0.21	6.3	12.61 ± 0.25	2.98 ± 1.01	1.08 ± 0.37	3.5	–	–	–	–	C
90110-02-01-00-3	11298,20354	3.72 ± 0.07	1.33 ± 0.26	1.51 ± 0.48	3.6	5.90 ± 0.04	0.81 ± 0.16	1.00 ± 0.19	6.0	12.41 ± 0.21	2.44 ± 0.68	0.64 ± 0.16	4.5	–	–	–	–	C
90110-02-01-02	*all*	3.30 ± 0.09	1.34 ± 0.32	2.05 ± 0.71	3.0	5.20 ± 0.02	0.53 ± 0.07	1.83 ± 0.22	8.2	11.21 ± 0.18	1.65 ± 0.44	0.71 ± 0.18	4.2	–	–	–	–	C
92035-01-03-01	*all*	1.18 ± 0.04	0.40 ± 0.10	1.33 ± 0.36	4.2	1.67 ± 0.00	0.12 ± 0.01	4.06 ± 0.22	18.1	3.34 ± 0.01	0.32 ± 0.02	2.84 ± 0.16	17.4	5.12 ± 0.08	0.65 ± 0.27	0.35 ± 0.12	3.2	C
92035-01-03-02	*all*	–	–	–	–	2.45 ± 0.00	0.14 ± 0.01	5.01 ± 0.21	23.4	4.94 ± 0.01	0.46 ± 0.07	1.15 ± 0.13	9.6	7.38 ± 0.07	0.59 ± 0.21	0.25 ± 0.08	3.4	C
92035-01-03-03	*all*	–	–	–	–	3.51 ± 0.01	0.29 ± 0.01	5.39 ± 0.18	31.7	7.10 ± 0.03	0.59 ± 0.07	0.83 ± 0.07	12.4	–	–	–	–	C
92035-01-03-05	*all*	3.03 ± 0.05	0.92 ± 0.25	1.02 ± 0.25	4.4	5.76 ± 0.02	0.59 ± 0.09	2.62 ± 0.57	4.8	11.49 ± 0.26	6.19 ± 0.73	2.30 ± 0.30	7.0	–	–	–	–	C
92428-01-04-00	*all*	2.13 ± 0.05	0.44 ± 0.12	0.65 ± 0.16	4.2	4.34 ± 0.01	0.42 ± 0.02	5.85 ± 0.17	33.3	8.78 ± 0.03	1.01 ± 0.11	1.17 ± 0.09	13.2	–	–	–	–	C
92428-01-04-01	*all*	2.04 ± 0.03	0.18 ± 0.12	0.38 ± 0.14	3.3	4.23 ± 0.01	0.37 ± 0.02	5.31 ± 0.21	25.3	8.50 ± 0.03	1.04 ± 0.11	1.37 ± 0.10	13.7	–	–	–	–	C
92428-01-04-02	*all*	2.16 ± 0.06	0.36 ± 0.16	0.46 ± 0.19	2.8	4.14 ± 0.01	0.40 ± 0.03	5.50 ± 0.25	22.7	8.37 ± 0.04	1.08 ± 0.14	1.21 ± 0.11	11.4	–	–	–	–	C
92428-01-04-03	*all*	2.53 ± 0.04	0.34 ± 0.13	0.60 ± 0.18	3.7	4.99 ± 0.01	0.49 ± 0.04	5.01 ± 0.21	24.7	10.08 ± 0.07	1.12 ± 0.30	0.92 ± 0.14	8.0	–	–	–	–	C
95409-01-14-03	*all*	–	–	–	–	1.59 ± 0.00	0.06 ± 0.02	2.61 ± 0.64	7.3	3.15 ± 0.01	0.17 ± 0.03	3.85 ± 0.33	11.3	–	–	–	–	C
95409-01-14-04	*all*	–	–	–	–	2.38 ± 0.01	0.10 ± 0.01	4.64 ± 0.37	12.3	4.77 ± 0.02	0.25 ± 0.05	1.09 ± 0.15	7.7	7.44 ± 0.13	2.11 ± 0.67	1.75 ± 0.45	4.5	C
95409-01-14-05	*all*	–	–	–	–	3.64 ± 0.01	0.23 ± 0.03	5.90 ± 0.40	15.3	7.37 ± 0.06	0.65 ± 0.13	1.05 ± 0.18	6.0	–	–	–	–	C
95409-01-14-06	*all*	–	–	–	–	2.42 ± 0.00	0.09 ± 0.01	4.52 ± 0.30	15.4	4.87 ± 0.02	0.29 ± 0.04	1.28 ± 0.12	11.0	7.27 ± 0.05	0.84 ± 0.21	0.98 ± 0.18	5.9	C
95409-01-14-07	*all*	1.92 ± 0.04	0.88 ± 0.18	2.35 ± 0.53	4.4	2.92 ± 0.00	0.15 ± 0.01	5.86 ± 0.21	28.3	5.93 ± 0.02	0.51 ± 0.06	0.83 ± 0.08	10.9	8.78 ± 0.03	0.54 ± 0.13	0.38 ± 0.05	7.4	C
95409-01-15-00	*all*	–	–	–	–	4.15 ± 0.01	0.33 ± 0.04	5.30 ± 0.31	17.0	8.36 ± 0.04	0.63 ± 0.13	0.95 ± 0.12	8.4	–	–	–	–	C
95409-01-15-01	*all*	2.83 ± 0.04	$0.22 \pm - 0.42$	0.25 ± 0.10	2.6	5.68 ± 0.02	0.50 ± 0.06	2.87 ± 0.20	14.6	11.81 ± 0.15	2.72 ± 0.61	1.05 ± 0.20	5.6	–	–	–	–	C
60705-01-84-02	*all*	–	–	–	–	4.97 ± 0.01	0.69 ± 0.02	5.72 ± 0.14	40.6	9.60 ± 0.07	1.49 ± 0.18	0.84 ± 0.07	12.0	–	–	–	–	B
70108-03-02-00	*all*	–	–	–	–	5.31 ± 0.01	0.51 ± 0.02	6.86 ± 0.18	37.8	10.56 ± 0.09	1.32 ± 0.22	0.65 ± 0.08	8.8	–	–	–	–	B
70109-01-07-00	*all*	–	–	–	–	5.90 ± 0.01	0.52 ± 0.01	4.20 ± 0.07	64.2	11.51 ± 0.05	1.48 ± 0.14	0.33 ± 0.02	15.5	–	–	–	–	B
70110-01-15-00	*all*	2.92 ± 0.05	0.37 ± 0.21	0.21 ± 0.08	2.5	5.81 ± 0.02	0.78 ± 0.04	5.02 ± 0.16	31.6	11.01 ± 0.48	4.09 ± 1.21	0.69 ± 0.13	6.6	–	–	–	–	B
90110-02-01-03	*all*	–	–	–	–	4.09 ± 0.01	0.47 ± 0.02	6.86 ± 0.24	29.2	8.03 ± 0.09	1.19 ± 0.24	0.80 ± 0.11	7.4	–	–	–	–	B
90704-01-02-00	*all*	–	–	–	–	4.21 ± 0.01	0.60 ± 0.03	6.61 ± 0.24	24.1	7.75 ± 0.47	3.72 ± 1.64	1.54 ± 0.38	4.9	–	–	–	–	B
92085-01-03-01	*all*	3.03 ± 0.03	0.30 ± 0.13	0.12 ± 0.04	3.7	6.20 ± 0.01	0.91 ± 0.03	3.75 ± 0.08	45.8	12.11 ± 0.10	1.43 ± 0.35	0.25 ± 0.04	6.1	–	–	–	–	B
95335-01-01-00	*all*	–	–	–	–	5.27 ± 0.01	0.66 ± 0.02	5.75 ± 0.12	48.3	10.48 ± 0.11	1.35 ± 0.27	0.54 ± 0.08	7.2	–	–	–	–	B
95335-01-01-01	*all*	–	–	–	–	5.09 ± 0.01	0.56 ± 0.01	4.58 ± 0.10	47.8	10.25 ± 0.08	1.29 ± 0.19	0.50 ± 0.05	9.6	–	–	–	–	B
95335-01-01-05	*all*	–	–	–	–	4.91 ± 0.01	0.51 ± 0.02	4.32 ± 0.13	33.8	9.72 ± 0.12	1.06 ± 0.35	0.33 ± 0.07	4.8	–	–	–	–	B
95335-01-01-07	*all*	–	–	–	–	5.32 ± 0.02	0.68 ± 0.03	5.99 ± 0.19	32.0	10.19 ± 0.14	1.41 ± 0.40	0.63 ± 0.11	5.9	–	–	–	–	B
95409-01-15-06	*all*	–	–	–	–	5.68 ± 0.01	0.47 ± 0.01	3.33 ± 0.09	38.5	11.09 ± 0.09	1.67 ± 0.28	0.30 ± 0.03	9.6	–	–	–	–	B
95409-01-17-05	*all*	–	–	–	–	5.23 ± 0.01	0.56 ± 0.02	4.43 ± 0.10	43.7	10.19 ± 0.10	1.28 ± 0.21	0.46 ± 0.05	8.6	–	–	–	–	B
95409-01-17-06	*all*	–	–	–	–	5.12 ± 0.02	0.57 ± 0.02	4.81 ± 0.16	29.9	10.14 ± 0.10	0.90 ± 0.30	0.39 ± 0.08	4.8	–	–	–	–	B
95409-01-18-00	*all*	–	–	–	–	5.38 ± 0.01	0.66 ± 0.02	5.46 ± 0.15	37.2	10.29 ± 0.15	2.46 ± 0.52	0.71 ± 0.09	8.1	–	–	–	–	B
95409-01-18-05	*all*	–	–	–	–	4.95 ± 0.02	0.50 ± 0.03	5.02 ± 0.25	20.4	9.53 ± 0.22	0.92 ± 0.38	0.40 ± 0.12	3.5	–	–	–	–	B
90110-02-01-01	*all*	2.69 ± 0.07	0.80 ± 0.42	1.78 ± 1.00	2.0	5.06 ± 0.03	0.37 ± 0.09	1.57 ± 0.36	4.5	11.37 ± 0.32	4.90 ± 1.36	3.34 ± 1.07	3.0	–	–	–	–	–
92035-01-03-06	*all*	2.86 ± 0.07	0.72 ± 0.22	0.53 ± 0.17	3.2	5.57 ± 0.01	0.77 ± 0.04	4.39 ± 0.14	29.4	11.24 ± 0.08	2.26 ± 0.35	0.95 ± 0.12	8.2	–	–	–	–	–
92428-01-04-04	*all*	2.90 ± 0.05	0.27 ± 0.17	0.28 ± 0.12	2.9	5.62 ± 0.01	0.72 ± 0.05	4.36 ± 0.19	24.1	11.35 ± 0.15	2.24 ± 0.57	0.72 ± 0.15	5.2	–	–	–	–	–
..	..	..	..	..	..	..	..	..	..	..	..	..	..	..	..	..	..	..

Table 3. Best-fit ratios for QPOs in Group 1 per source. Errors quoted use $\Delta\chi^2 = 9$ (3σ 1-parameter error).

Source	QPO pair	#Maps	Best-fitting a (3σ)	χ^2/d.o.f.
GX 339–4	QPO_1,QPO_2	49	$2.011^{+0.005}_{-0.006}$	20801/16050
	$QPO_{\frac{1}{2}}$,QPO_1	32	1.945 ± 0.004	16051/10490
	QPO_1,QPO_3	4	3.009 ± 0.009	1460/1289
GRO J1655–40	QPO_1,QPO_2	16	$2.01^{+0.03}_{-0.01}$	6209/5455
4U 1630–47	QPO_1,QPO_2	2	2.06 ± 0.08	868/719
XTE J1550–564	QPO_1,QPO_2	63	$1.975^{+0.002}_{-0.003}$	30547/20366
	$QPO_{\frac{1}{2}}$,QPO_1	46	1.995 ± 0.004	23645/14698
	QPO_1,QPO_3	4	$3.022^{+0.01}_{-0.07}$	2024/1386
H 1743–322	QPO_1,QPO_2	52	$1.988^{+0.005}_{-0.003}$	21252/17354
	$QPO_{\frac{1}{2}}$,QPO_1	22	$2.04^{+0.03}_{-0.02}$	9778/7153
	QPO_1,QPO_3	8	3.01 ± 0.03	3126/2663

3.1 Fits to QPO relations in Group 1

We report the best-fitting proportionality constants (a) to the various frequency–frequency relations of QPOs in Group 1 for each source in Table 3 measured using the method of van Doesburgh & van der Klis (2017) (see Section 2).

We provide plots of the significances of the residuals to each fit, which we calculate directly from the χ^2 contributions of each point to the overall χ^2 of the fit, using confidence levels appropriate to 2 parameters such that the 2σ (= 95.4 per cent) confidence level, for instance, corresponds to a χ^2 contribution of 6.17. In Figs 2(c), 3(c), 4(c), 5(c), and 6(c), we combine the residuals of the frequency–frequency fits in one plot per source. In Fig. 7(a), we plot the frequency ratios ν_3/ν_2, ν_2/ν_1, $\nu_1/\nu_{\frac{1}{2}}$ versus the frequency of QPO_1 for Group 1 with single parameter 1σ-errors, which for the ratios were obtained by standard error propagation. (In this figure we use less conservative error bars as we are only interested in displaying general trends of the QPO frequency ratios.) A histogram of this plot is shown in Fig. 8(a).

We find small but very significant offsets (in some cases $>40\sigma$) from integer proportionality constants (a). A careful analysis of how these offsets arise suggests that the main cause is the presence of frequency pairs with small error bars contributing a highly significant non-integer frequency ratio. These show up in the residual plots as the $\gtrsim 3\sigma$ deviations. Indeed, although the reduced χ^2 values of the fits are all <1.6, in view of the high number of degrees-of-freedom (which arise as we fit all power spectra simultaneously to measure the frequency relations, see van Doesburgh & van der Klis 2017) many of these χ^2 values are formally unacceptable. We further investigate QPO pairs causing notable outliers for each source in the Appendix. We conclude that in the majority of cases they can be explained by the shape of a Lorentzian not matching the QPO peak perfectly. Mostly, this applies to QPOs classified as Type B in earlier works which show little broad-band noise. We use a broad energy band in this work, and as it is known that the QPO frequency can depend on energy (van den Eijnden, Ingram & Uttley 2016), further study is needed to accurately quantify this effect. In some power spectra, however, (mostly seen for GX 339–4), the centroid frequency of the sub-harmonic clearly is significantly higher than expected while there is no sign of an ill-fitting Lorentzian. Their $\nu_1/\nu_{\frac{1}{2}}$ frequency ratios are $\sim$1.5, and stand out from others at $\sim$2 (see Fig. A3). The sub-harmonic peaks are relatively weak and have low Q ($Q \sim 2.5$), which means their centroid frequencies could have been affected by blends with other low-frequency features. These QPO pairs are the main reason for the extreme deviation from an integer proportionality of the $QPO_{\frac{1}{2}}$, QPO_1 relation in GX 339–4 (see Appendix A).

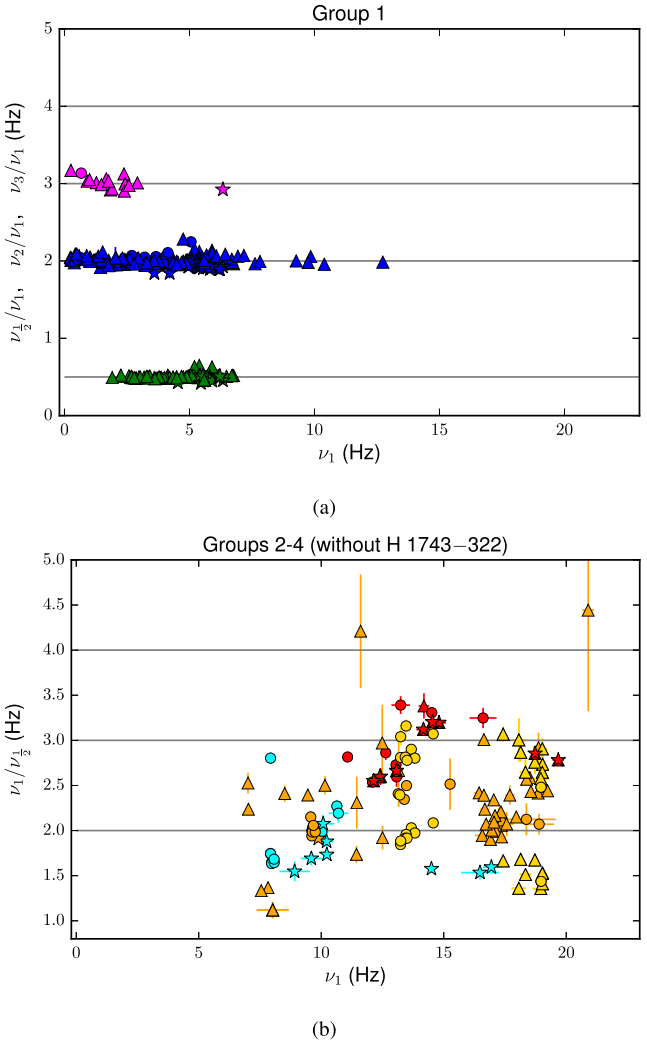

Figure 7. (a) QPO frequency ratios (ν_3/ν_1 plotted in *magenta*, ν_2/ν_1 plotted in *blue*, and $\nu_{\frac{1}{2}}/\nu_1$ plotted in *green*) in Group 1. Integer frequency ratios are indicated with *grey* horizontal lines. Errors use $\Delta\chi^2 = 1$, the error on the ratio assumes uncorrelated errors on the frequencies. (b) As in panel (a) but with $\nu_1/\nu_{\frac{1}{2}}$ in Group 2 (plotted in *cyan*), Group 3 (plotted in *orange*), Group 3a (plotted in *yellow*, the two frequencies of $QPO_{\frac{1}{2}}$ are both included), and Group 4 (plotted in *red*) versus ν_1.

3.2 Frequency ratios in Groups 2–4

Simultaneous QPOs and peaked noise in Groups 2, 3, 3a, 4 are clearly not at integer frequency ratios, as evidenced by the significant deviations from them in Figs 2(a), 3(a), 4(a), 5(a), and 6(a).

As in Figs 7(a), in 7(b) we plot the frequency ratios $\nu_1/\nu_{\frac{1}{2}}$ versus the frequency of QPO_1, and use both the high and LF of the 'jumping' QPO in Group 3a. A histogram of this plot is shown in Fig. 8(b).

We find that Group 4 power spectra, which are seen for GRO J1655–40, 4U 1630–47, XTE J1550–564, and H 1743–322 have QPOs with frequency ratios larger than 2, and close to 3, and that can vary for a given source (e.g. 4U 1630–47).

The frequencies of the QPOs in Group 3a (*yellow*) for 4U 1630–47, with $\nu_1 \sim 13.5$ Hz, are a factor $\sim$2 and $\sim$3 lower than of QPO_1. Those in Group 3a for GRO J1655–40 are a factor $\sim$1.5 and $\sim$2.5 lower than of QPO_1 with $\nu_1 \sim 18$ Hz. For both sources, the variable low-frequency QPO therefore changes by a factor $\sim$1.5. The Group

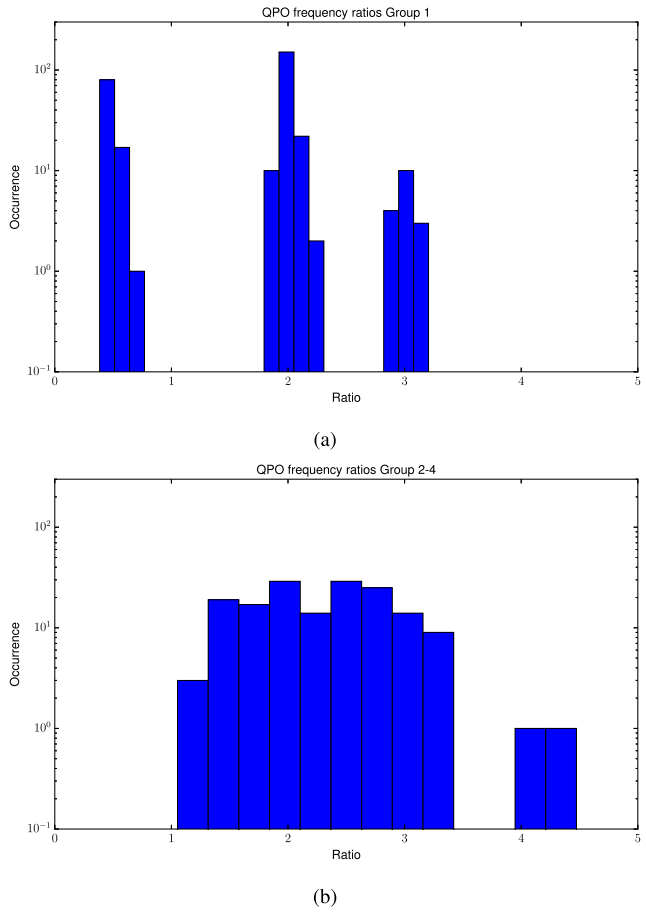

Figure 8. Number histograms of frequency ratios displayed in Figs 7(a) and (b).

3 (*orange*) peaked noise frequency occurs at the average of the two QPO frequency factors for these sources, at about half the frequency of the >10 Hz QPO.

The majority of the QPOs in Group 2 (*cyan*) have frequency ratios that are slightly lower than 2. For H 1743–322, we have many detections of Group 2 power spectra that clearly form a homogeneous and separate group from the other power spectra with multiple QPO seen for this source. We plot the frequency ratio of these Group 2 QPOs separately in Fig. 9, versus the frequency of $\mathrm{QPO}_{\frac{1}{2}}$. As can be seen in Fig. 6(a), $\mathrm{QPO}_{\frac{1}{2}}$ is not a single-valued function of QPO_1, which is why in this case we use the frequency of $\mathrm{QPO}_{\frac{1}{2}}$ on the *x*-axis. Clearly, for this source, the frequency ratio systematically decreases with QPO frequency. We note that the 'cathedral' QPOs in XTE J1859+226 (a source not included here, but which QPOs we would categorize as Group 2) were previously reported by Rodriguez & Varnière (2011) to be not harmonically related based on a lack of bi-coherence and differences in QPO characteristics.

QPO_1 does not have detectable harmonics at higher frequency in Groups 2–4. The 99 per cent confidence upper limits on a QPO_2 with similar Q as QPO_1 are better than ∼2 per cent rms (up to 1 per cent rms) in Groups 2–3 and up to ∼0.4 per cent rms in Group 4.

4 DISCUSSION AND CONCLUSION

Through a systematic comparative analysis of simultaneous LF-QPOs (0.1–30 Hz) in a sample of five BH-LMXBS we find that when focusing on QPO multiplicity, these QPOs present a rather different picture from the one obtained by casual inspection of the power spectra. We find there is an extensive set of observations with very similar power spectra, which we have designated Group 1 in this work, where the QPOs show up in the form of a set of harmonically related power spectral peaks, previously classified as Type B or Type C depending on the amount of broad-band noise underlying the QPO peaks. In addition to this, multiple QPOs occur in a much more varied set of observations whose power spectra, designated Groups 2–4 here, present a superficially similar picture of a set of 2 or 3 simultaneous QPO peaks in the 0.1–30 Hz range on top of various broad noise, but here closer scrutiny shows the peaks are not in fact harmonically related: their frequency ratios occur anywhere in the range ∼1–3.5 with no preference for integer frequency ratios.

In the Group 1 power spectra, which occur in the hard/hard-intermediate state, simultaneous QPOs have integer frequency ratios indicating a common physical origin for which precession is a viable candidate (as discussed in the Section 1).

Offsets from purely integer ratios are mostly caused in this group by ill-fitting Lorentzian fit functions. We do however find some cases where the sub-harmonic has significantly higher than expected frequency; an analysis comparing the QPO shape and frequency in short time segments and multiple energy bands is required to quantify these results further (e.g. van den Eijnden et al. 2016).

The shifts from purely integer frequency ratios predicted by oscillation mode models (e.g. Titarchuk 2002; Varnière et al. 2012) are not observed to occur in any systematic way in Group 1. In a given power spectrum, we do not detect offsets for all harmonics, and the offsets we do observe cannot be systematically linked to the QPO parameters.

Explaining the multiple QPOs with non-integer frequency ratios in Groups 2–4 (that are clearly not caused by imperfect fits like the outliers in Group 1) within a single model framework, such as precession (Ingram et al. 2009) or intrinsic flow variability (Titarchuk 2002; Varnière et al. 2012), is challenging. These models predict integer, and near-integer QPO frequency ratios, respectively, where instead we find significant and in some cases systematically varying non-integer frequency ratios. Simultaneous corrugation and pressure modes (e.g. Wagoner et al. 2001) could have unrelated frequencies, but are expected to have very different amplitudes, which is at odds with the QPOs we detect. A scenario that might perhaps account for simultaneous non-harmonic QPOs is that of disc-tearing seen in GRMHD simulations (Liska et al. 2020). Inner and outer parts of the disc can precess with different frequencies in this context. We note that as the Group 2–4 QPOs are observed mainly in high-inclination sources (see Motta et al. 2015 and references therein) and not the low-inclination source GX 339–4, the edge-on viewing angle of the flow might enhance physical effects that are not seen for low-inclination sources.

Taking one step back from trying to apply specific models, it is useful to state a few general considerations that should apply to any interpretation of this rather complex QPO phenomenology. As all simultaneous QPOs occur in the 0.1–30 Hz range, it needs to be considered if one or both of the two simultaneous QPO peaks at non-integer frequency ratios in Groups 2–4 (where we assume one QPO underlies the two 'jumping' QPOs in Group 3a) are similar to those in Group 1, where 2–4 peaks are seen at integer frequency ratios. If both peaks the same as Group 1 QPOs, then there must be a mechanism that shifts the peaks away from the harmonic relations seen for Group 1. In a precession model that mechanism might be propagating warps (van den Eijnden et al. 2016). Additionally, something must prevent more than two peaks to show up.

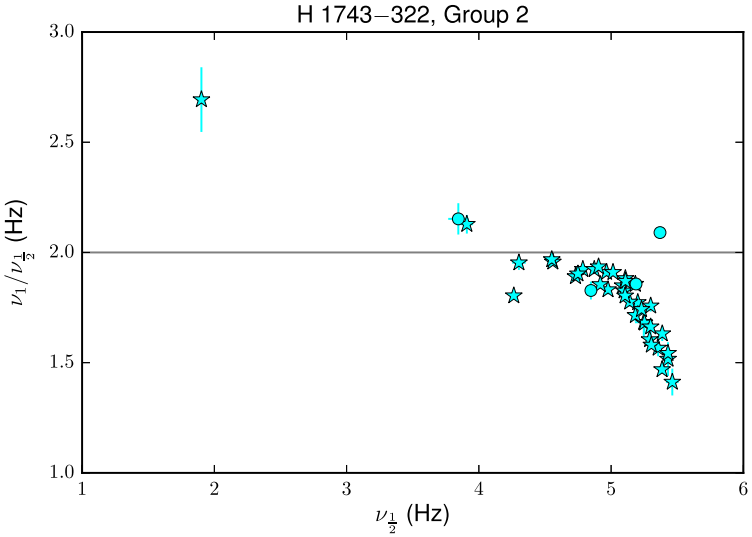

Figure 9. Frequency ratio of Group 2 QPO_1 with $\mathrm{QPO}_{\frac{1}{2}}$ in H 1743–322 versus $\nu_{\frac{1}{2}}$. A frequency ratio of 2 is indicated with a *grey* horizontal line. Errors use $\Delta\chi^2 = 1$, the error on the ratio assumes uncorrelated errors on the frequencies.

If one of the peaks is a Group 1 QPO but the other is not, then a second mechanism is needed beyond the mechanism responsible for Group 1 QPOs that somehow produces a QPO peak that is rather similar to the other peak but does not operate in Group 1. Additionally in this scenario something must prevent harmonics of the Group 1 QPO to show up.

If, finally, both peaks in Groups 2–4 are different from those in Group 1, then somehow the mechanism producing the QPOs in Group 1 is prevented from operating in Groups 2–4. We would need one or two additional mechanisms that do not operate in Group 1 to produce the two non-harmonic QPOs.

Any additional mechanism producing the QPOs in Groups 2–4 could also be responsible for the higher-than-expected sub-harmonics in Group 1. Of course, the QPOs in Groups 2–4 could also have different origins from group to group. Any combination of the models mentioned earlier could underly these scenarios, with the explicit requirement that in some of them, the QPOs lack harmonics.

All of the suggested schemes have consequences for the A/B/C classifications of the QPOs in Groups 2–4. In particular, lumping some of these Group 2–4 QPOs with the B/C QPOs of Group 1 may be misleading: their lack of harmonics and occurrence with a non-harmonic companion suggests a different underlying mechanism.

Future work includes analyses of simultaneous LF QPOs in sources not featured in this work. Additionally, it would be interesting to perform a detailed spectral-timing analysis of the different QPOs to further investigate the phenomenological grouping scheme we propose. Also, if in the future the number of detections of simultaneous QPOs at high (>100 Hz) and LF increases, it would be interesting to study frequency–frequency correlations and compare them to model predictions and those seen in NS-LMXBs.

ACKNOWLEDGEMENTS

This research has made use of data obtained through the High Energy Astrophysics Science Archive Research Center Online Service, provided by the NASA/Goddard Space Flight Center. This work is (partly) financed by the Netherlands Organisation for Scientific Research (NWO).

DATA AVAILABILITY

The raw RXTE data used in this paper can be found at NASA's High Energy Astrophysics Science Archive Research Center (HEASARC): heasarc.gsfc.nasa.gov. All results obtained from our analysis can be found, as stated in the caption of Table 2, at: https://github.com/mariekevandoesburgh/harmonics.

REFERENCES

Belloni T. M., Motta S. E., 2016, Transient Black Hole Binaries. Springer-Verlag, Berlin, Heidelberg, p. 61
Casella P., Belloni T., Stella L., 2005, ApJ, 629, 403
Choudhury M., Bhatt N., Bhattacharyya S., 2015, MNRAS, 447, 3960
de Ruiter I., van den Eijnden J., Ingram A., Uttley P., 2019, MNRAS, 485, 3834
Dieters S. W. et al., 2000, ApJ, 538, 307
Gao H. Q. et al., 2017, MNRAS, 466, 564
Homan J., Wijnands R., van der Klis M., Belloni T., van Paradijs J., Klein-Wolt M., Fender R., Méndez M., 2001, ApJS, 132, 377
Homan J., Miller J. M., Wijnands R., Lewin W. H. G., 2005a, American Astronomical Society Meeting Abstracts. American Astronomical Society, USA, p. 102.01
Homan J., Miller J. M., Wijnands R., van der Klis M., Belloni T., Steeghs D., Lewin W. H. G., 2005b, ApJ, 623, 383
Ingram A., Motta S., 2020, preprint (arXiv:2001.08758)
Ingram A., Done C., Fragile P. C., 2009, MNRAS, 397, L101
Ingram A., van der Klis M., Middleton M., Done C., Altamirano D., Heil L., Uttley P., Axelsson M., 2016, MNRAS, 461, 1967
Kalamkar M., Casella P., Uttley P., O'Brien K., Russell D., Maccarone T., van der Klis M., Vincentelli F., 2016, MNRAS, 460, 3284
Klein Wolt M., 2004, PhD thesis. University of Amsterdam
Li Z. B., Gao H. Q., Zhang Z., Zhang S., Qu J. L., Zhang C. M., Song L. M., 2014, MNRAS, 440, 143
Liska M., Hesp C., Tchekhovskoy A., Ingram A., van der Klis M., Markoff S. B., Van Moer M., 2020, MNRAS, preprint (arXiv:1904.08428)
Miyamoto S., Kimura K., Kitamoto S., Dotani T., Ebisawa K., 1991, ApJ, 383, 784
Motta S., Muñoz-Darias T., Casella P., Belloni T., Homan J., 2011, MNRAS, 418, 2292

Motta S., Homan J., Muñoz Darias T., Casella P., Belloni T. M., Hiemstra B., Méndez M., 2012, MNRAS, 427, 595
Motta S. E., Belloni T. M., Stella L., Muñoz-Darias T., Fender R., 2014a, MNRAS, 437, 2554
Motta S. E., Munoz-Darias T., Sanna A., Fender R., Belloni T., Stella L., 2014b, MNRAS, 439, L65
Motta S. E., Casella P., Henze M., Muñoz-Darias T., Sanna A., Fender R., Belloni T., 2015, MNRAS, 447, 2059
Nespoli E., Belloni T., Homan J., Miller J. M., Lewin W. H. G., Méndez M., van der Klis M., 2003, A&A, 412, 235
Remillard R. A., Sobczak G. J., Muno M. P., McClintock J. E., 2002, ApJ, 564, 962
Rodriguez J., Varnière P., 2011, ApJ, 735, 79
Schnittman J. D., Homan J., Miller J. M., 2006, ApJ, 642, 420
Stella L., Vietri M., 1998, ApJ, 492, L59
Tagger M., Pellat R., 1999, A&A, 349, 1003
Titarchuk L., 2002, ApJ, 578, L71
Titarchuk L., Lapidus I., Muslimov A., 1998, ApJ, 499, 315
Trudolyubov S. P., Borozdin K. N., Priedhorsky W. C., 2001, MNRAS, 322, 309
van den Eijnden J., Ingram A., Uttley P., 2016, MNRAS, 458, 3655
van der Klis M., 1989, in Ögelman H., van den Heuvel E. P. J., eds, NATO Advanced Science Institutes (ASI) Series C Vol. 262, NATO Advanced Science Institutes (ASI) Series C. Springer, Dordrecht, p. 27
van Doesburgh M., van der Klis M., 2017, MNRAS, 465, 3581
van Straaten S., van der Klis M., di Salvo T., Belloni T., 2002, ApJ, 568, 912
Varnière P., Tagger M., Rodriguez J., 2012, A&A, 545, A40
Wagoner R. V., Silbergleit A. S., Ortega-Rodríguez M., 2001, ApJ, 559, L25
Wijnands R., Homan J., van der Klis M., 1999, ApJ, 526, L33
Zhang W., Jahoda K., Swank J. H., Morgan E. H., Giles A. B., 1995, ApJ, 449, 930

APPENDIX A: DETAILS OF THE ANALYSIS

Here, we report details of our analysis per source. In Figs A2, A8, A10, A12, and A17, we plot the fractional rms (added in quadrature for all QPOs and the peaked noise components in Group 3 in the power spectrum) versus QPO_1. We note that the errors on the combined fractional rms values are overestimated, as we assume the errors on the fractional rms of the different power spectral components to be uncorrelated. The added fractional rms of the QPOs in Group 2 (plotted in *cyan*) stands apart by being notably lower than that of those in Group 1 (plotted in *blue*), supporting our categorization. For XTE J1550–564 however, this subdivision is not as clear.

GX 339–4

In Fig. A1, we show typical power spectra for GX 339–4 that contain multiple QPOs.

Note that Group 1 includes power spectra with little broad-band noise, see bottom right panel of Fig. A1, identified as Type B in earlier works as well as power spectra with strong noise where the QPOs were identified as Type C. Following (Motta et al. 2011), we only use the segments of observations 70109-01-07-00 and 70108-03-02-00 where we can detect multiple QPOs, discarding the segments where a single Type A QPO is reported.

We find observations with double QPOs in the soft state with frequency ratios (∼2.2) 70109-01-19-00, 70130-01-01-00, and 92085-01-01-05, see the top right panel of Fig. A1. Although the frequency ratios for the QPOs in these observations are formally consistent with integers (within 3σ), we categorize these QPOs as belonging

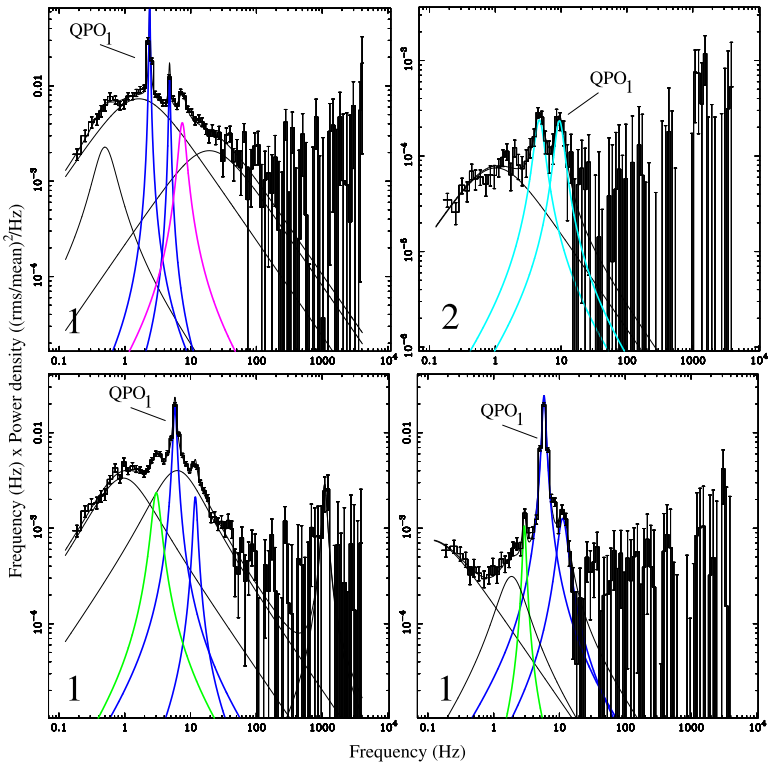

Figure A1. Characteristic power spectra for BH GX 339–4. The observations used are in a clockwise direction from the top left: 95409-01-14-04 (Group 1) and 70109-01-19-00 (Group 2) and 60705-01-84-02 (Group 1) and 70110-01-11-00 (Group 1). Note the different *y*-axis values.

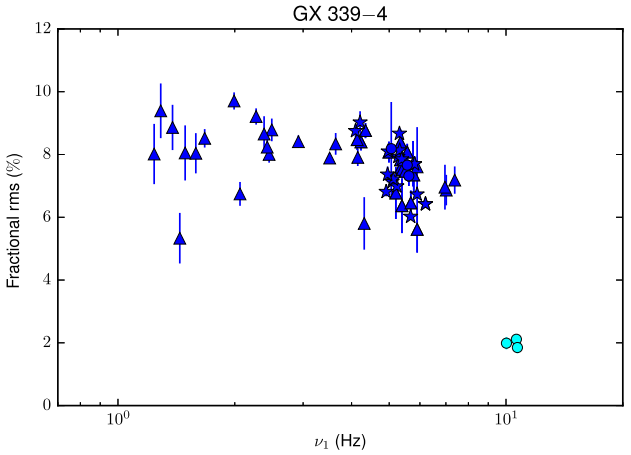

Figure A2. Fractional rms versus QPO_1 for GX 339-4. Colours correspond to those used in Fig. 2(a).

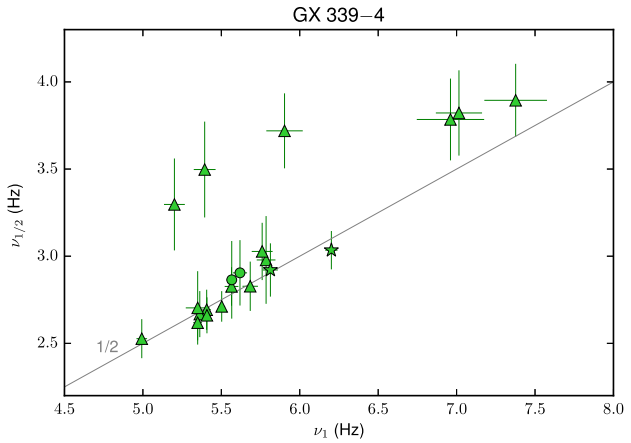

Figure A3. Zoom-in of Fig. 2(a).

to Group 2 as their low Q and comparable fractional rms amplitudes are compatible with Group 2 QPOs.

We further investigate notable outliers to the best proportionality ratio fits seen in Fig. 2(c).

The QPO pairs in *green* with QPO_1 ∼5 Hz and $QPO_{\frac{1}{2}}$ ∼3 Hz are fitted power spectra of observations 90110-02-01-02, 90110-02-01-00 (two segments), 92085-01-03-00, 92085-01-03-03, and 92085-01-03-02. We show a zoom of Fig. 2(a) in Fig. A3 in the relevant frequency range, the error bars indicate the extremes of the 2-parameter 99 per cent confidence contour. In Fig. A4, we plot the fit and residuals of the power spectrum of observation 90110-02-01-02 indicating the centroid frequency of the expected (with $\nu_{\frac{1}{2}} = 0.5\nu_1$) and best-fitting sub-harmonic with black arrows. The choice of fit function does not seem to be the cause of a non-harmonic frequency ratio; the sub-harmonic and fundamental are well fitted with Lorentzians.

Omitting these two frequency pairs from the fit of all QPO_1, $QPO_{\frac{1}{2}}$ maps, we obtain a 1.994 ± 0.015 (3σ error) 9116/7605 (χ^2/dof) fit, the frequency pairs underlying the 3σ outliers at ∼2 Hz now no longer contribute high $\Delta\chi^2$ to the best-fitting ratio. The Type B residuals of the best-fitting QPO_2, QPO_1 proportionality are systematically negative. We use observation 91085-01-03-01 with $\nu_1 \sim 6.1$ Hz as a test case to investigate further; both the sub-harmonic and the harmonic have similar negative ∼3σ residuals which implies the

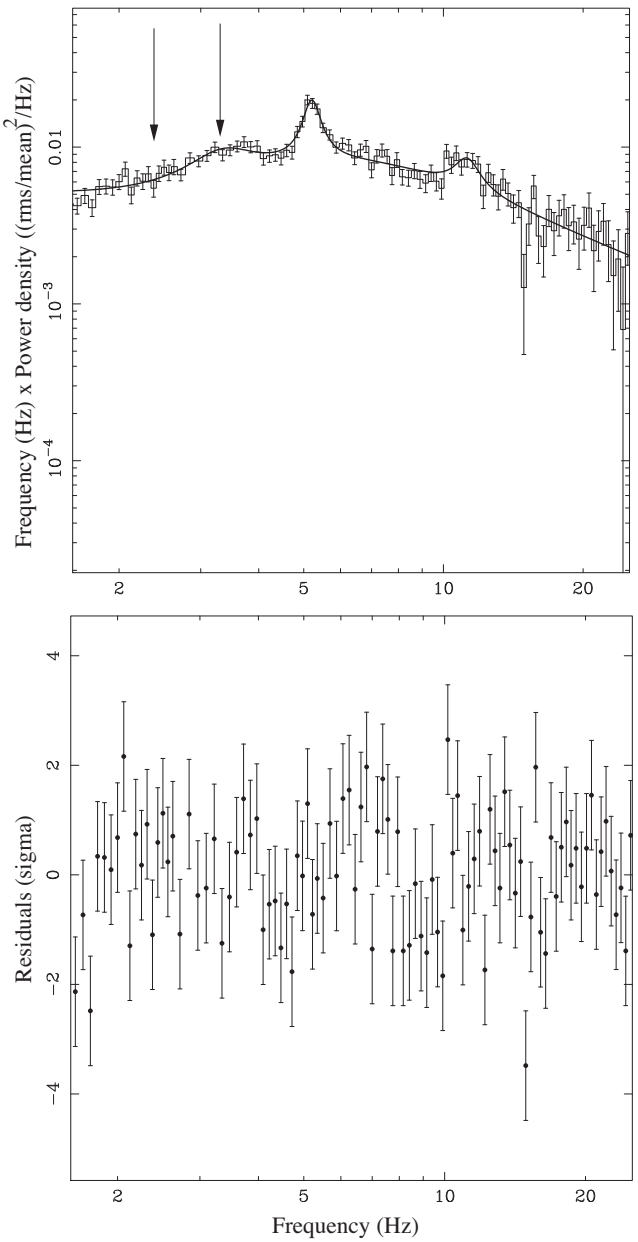

Figure A4. Fit and residuals to GX 339–4 observation 90110-02-01-02. The centroid frequency of the best-fitting sub-harmonic is indicated with the arrow at $\nu_{\frac{1}{2}} = 3.30 \pm 0.01$, the expected sub-harmonic centroid frequency of exactly half the fundamental frequency $\nu_{\frac{1}{2}} = 2.6$ is indicated with the leftmost arrow.

sub-harmonic is too far below QPO_1 and the second harmonic is not far enough above it. In Fig. A5, we plot the fit and residuals of the power spectrum. The fit function does not describe the data well. It seems likely that with a slightly lower QPO_1 frequency, which might be achieved with a different fit function, the frequency ratios with the harmonic and sub-harmonic could be reconciled with being 2 and 0.5, respectively. A similar conclusion was drawn by Nespoli et al. (2003) for the ∼6 Hz QPO in observation 70109-01-07-00; the authors find that a better fit to the QPO is obtained with a Gaussian + Lorentzian, yielding a slightly lower centroid frequency than with a Lorentzian fit.

The ∼3σ positive residuals at ∼5.5 Hz are caused by an ill-fitting QPO_2 Lorentzian that overestimates the frequency. As an example of

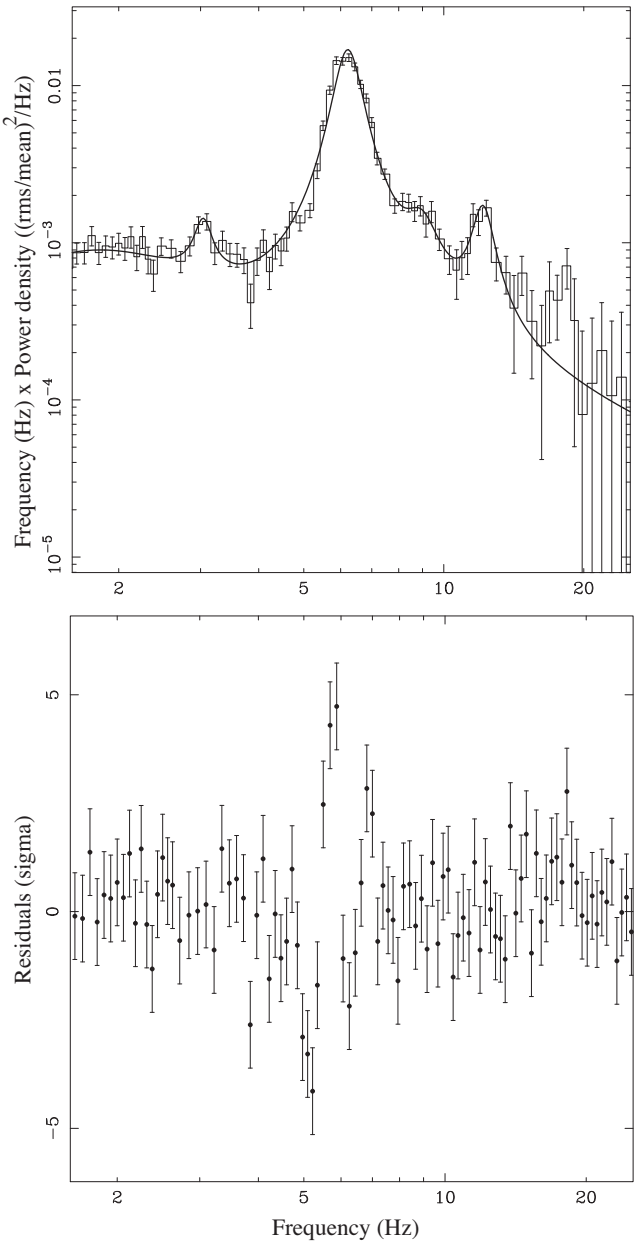

Figure A5. Fit and residuals to GX 339–4 observation 92085-01-03-01. A Lorentzian does not perfectly describe QPO_1 with $\nu_1 = 6.20 \pm 0.01$ Hz. Note how the right wing of the central QPO is fitted with an extra Lorentzian at ∼8Hz.

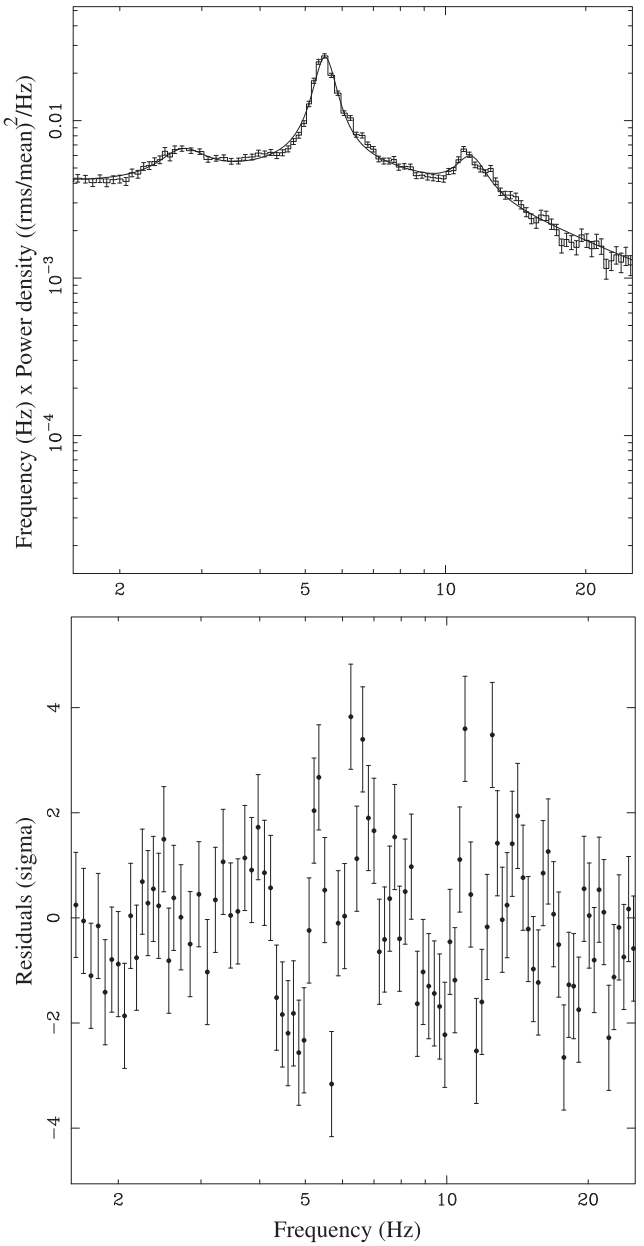

Figure A6. Fit and residuals to GX 339–4 observation 70109-04-01-01. A Lorentzian does not perfectly describe QPO_2 with $\nu_1 = 11.29 \pm 0.05$ Hz, the frequency is overestimated.

this, in Fig. A6 we plot an example for observation 70109-04-01-01 (with a time selection between 5000-15000s), which causes a 2.9σ outlier.

GRO J1655–40

In Fig. A7, we show representative power spectra of the groups we encounter for this source. We rely on both Motta et al. (2014a, 2015) for the identification of QPOs as Type B or Type C. Some QPOs were reported to have a sub-harmonic in Motta et al. (2014a, 2015) with $\nu_{\frac{1}{2}}$ ∼0.05–0.15 Hz. These features have low signal-to-noise ratio; we do not detect them at $>2\sigma$. For observation 91702-01-80-01, we reject the first third of the observation, during which no harmonic is detected.

All four groups of power spectra are seen for GRO J1655–40. The residuals of the best-fitting ratios plotted in Fig. 3(c) all fall within 3σ. The fit to the power spectrum causing the $\sim 2\sigma$ outlier near $\nu_1 = 10.4$ Hz describes the data well.

4U 1630–47

Representative power spectra of the groups we encounter for this source are shown in Fig. A9. As mentioned in the main text, Dieters et al. (2000) investigated the power spectra in Group 3a in detail. They conclude that in addition to the ∼13.5 Hz QPO, only one QPO is present with variable frequency that is related to dips in the light

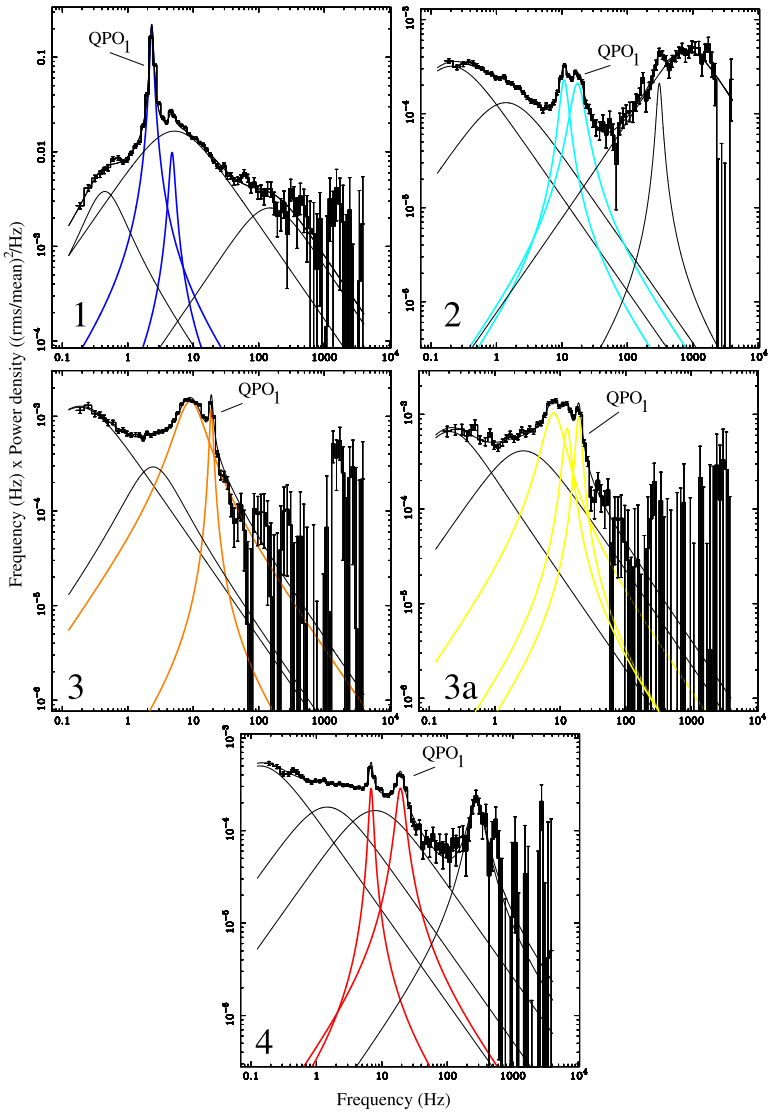

Figure A7. Characteristic power spectra for GRO J1655–40. The observations used are: 90704-04-01-00 (Group 1), 10255-01-05-00 (Group 2), 91702-01-59-02 (Group 3), 91702-01-58-03 (Group 3a), and 91702-01-58-00 (Group 4).

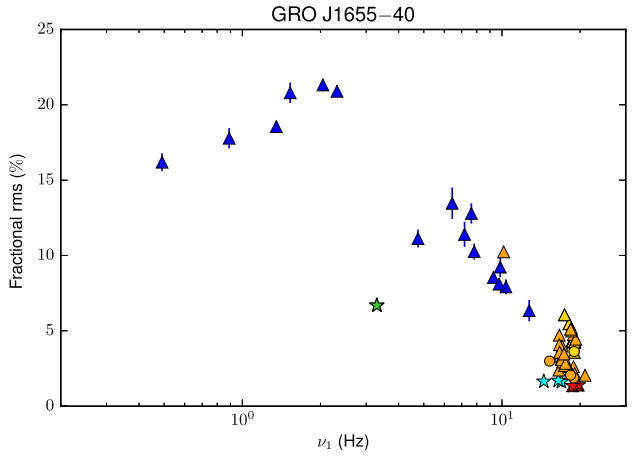

Figure A8. Fractional rms versus QPO_1 for GRO 1655. Colours and symbols correspond to those used in Fig. 3(a).

curve. The QPO frequency moves from 4–6 to 6–8 Hz. We categorize all power spectra with a QPO at ∼13.5 Hz as belonging to Group 3a. Several observations (30188-02-03-00, 30188-02-04-00, 30178-02-01-01, 30178-01-03-00, 30188-02-02-00, 30172-01-01-03, and 30188-02-01-00) contain two QPOs with lower Q and fractional rms than the QPOs in Group 1 (by a factor 2) setting them apart from that group. In observation 30188-02-02-00, we fit an additional sub-harmonic QPO at ν ∼2.8 Hz. The frequencies of ∼5 and ∼8 Hz QPOs in four of these observations are less than a factor 2 apart, similar to Group 2 power spectra, but in a few of the observations the QPOs are at integer frequency ratios. We categorize these power spectra as Group 2.

XTE J1550–564

In Fig. A11, we show representative power spectra of the four groups we encounter for XTE J1550–564. In addition to those reported in Motta et al. (2014b) we use identifications of Type B and Type C QPOs reported in Remillard et al. (2002), where the timing and

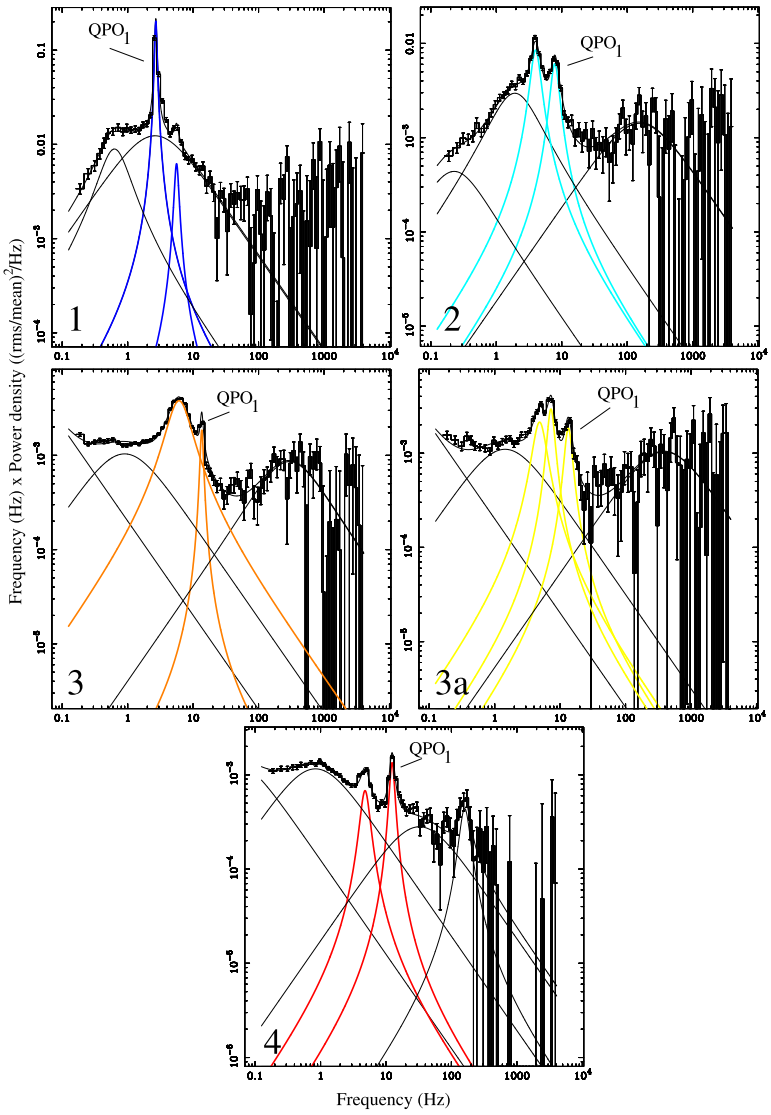

Figure A9. As in Fig. A1, but for 4U 1630–47. The observations used are in a clockwise direction from the top left: 30178-02-01-00 (Group 1), 30188-02-02-00 (Group 2), 30178-02-02-01 (Group 3a), 80117-01-05-00 (Group 4), and 30178-01-10-00 (Group 3).

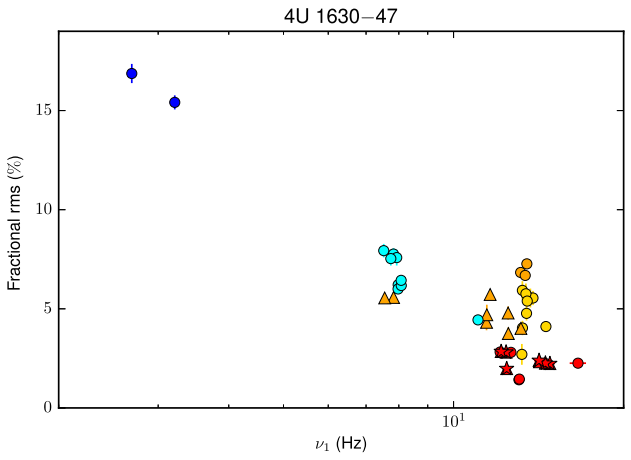

Figure A10. Fractional rms versus QPO_1 for 4U 1630-47. Colours correspond to those used in Fig. 4(a).

spectral behaviour of XTE J1550–564 are extensively reported using 209 RXTE observations from 1998–1999. When two conflicting identifications of QPOs exist between Motta et al. (2014b) and Remillard et al. (2002) (type A in Remillard et al. 2002 is Type B in Motta et al. 2014b), we use those reported in Motta et al. (2014b).

QPOs classified as Type A-1 in Wijnands et al. (1999) and Homan et al. (2001) were later identified as Type B Casella et al. (2005); we use that latter identification.

For observation 70109-01-19-00 we only use that part of the observation where multiple QPOs are seen. Representative power spectra of Groups 1, 2, and 4 are shown in Fig. A11. No Group 3 or 3a power spectra were found for XTE J1550–564.

We investigate notable outliers in Group 1 from the best proportionality fit further (see Fig. 5c). In observation 50134-02-01-01 (with QPO_1 at ∼4 Hz and QPO_2 at ∼8 Hz), we overestimate the power in the lower half of QPO_2 by fitting it with a Lorentzian. This results in the negative residuals around ∼7 Hz in Fig. A13: the fit function does not match the data perfectly. This is also true for the outliers in observation 50134-01-05-00 (with $\nu_1 = 4.48 \pm 0.01$ Hz)

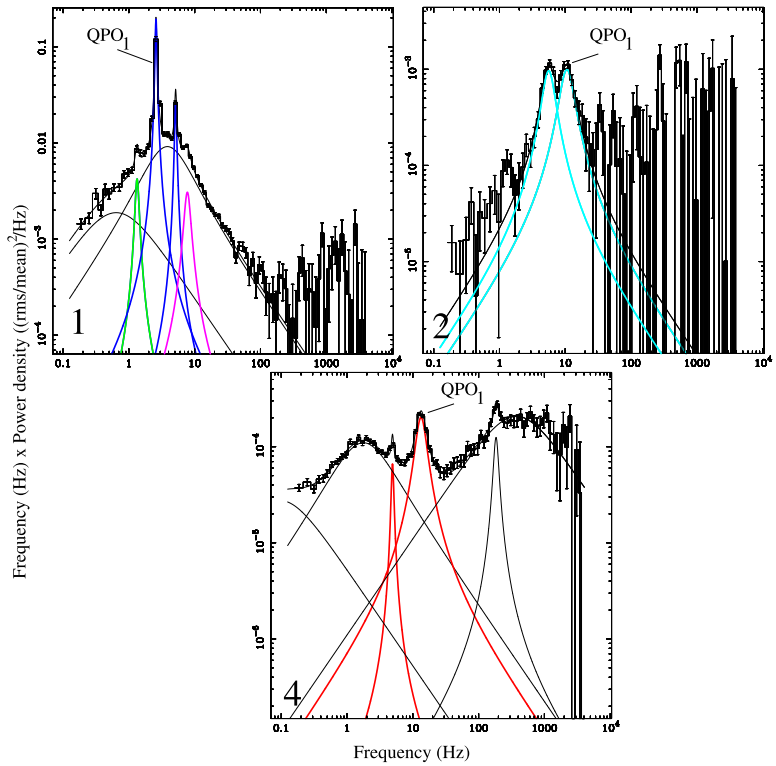

Figure A11. As in Fig. A1, but for XTE J1550. The observations used are in a clockwise direction from the top left: 30188-06-10-00 (Group 1), 40401-01-61-00 (Group 2), and 30191-01-02-00 (Group 4).

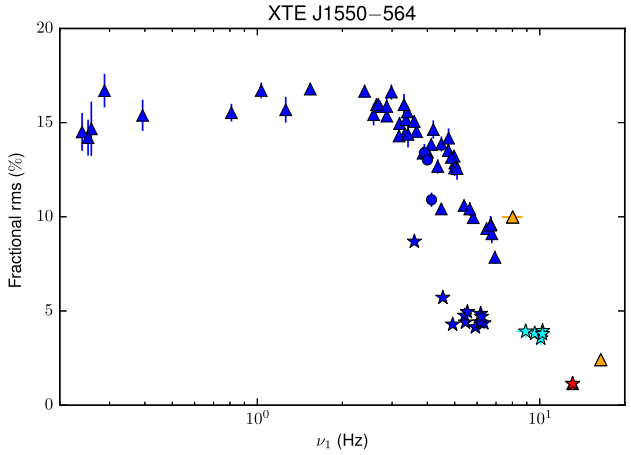

Figure A12. Fractional rms versus QPO_1 for XTE J1550. Colours and symbols correspond to those used in Fig. 5(a).

30191-01-29-00 (with $\nu_1 = 4.86 \pm 0.01$ Hz), 30188-06-01-03 (with $QPO_1 = 1.033 \pm 0.003$ Hz). In observation 30191-01-31-01 (with $\nu_1 = 6.75 \pm 0.01$Hz), we find a sub-harmonic at slightly higher frequency (with $>3\sigma$) than expected (with $\nu_{\frac{1}{2}} = 3.49 \pm 0.03$, analogous to the two cases we encountered for GX 339–4 (see Fig. A4). We plot the fit and residuals in Fig. A14, the residuals show no sign of a bad fit.

As a representative power spectrum of those containing the QPOs causing the negative outliers at ∼6 Hz (indicated with *stars*, Type B) we investigate observation 40401-01-55-00 further. We find that a Lorentzian does not match the shape of QPO_1, see Fig. A15. Adding an extra narrow component does not improve the fit, the wings of the QPO and the QPO remain ill-fitted. By using a Lorentzian we appear to overestimate the centroid frequency of the QPO, causing deviations for the (sub-)harmonics from the best-fitting ratio with QPO_1. In Wijnands et al. (1999), Remillard et al. (2002), and Homan et al. (2001) a similar conclusion was drawn for other observations with similar power spectra.

H 1743–322

In Fig. A16, we show representative power spectra of the four groups we encounter for H 1743–322. Our Group 2 power spectra all resemble the power spectrum of 'observation 2' by Homan et al. (2005b). In that work, the authors show that the power spectrum changes throughout this observation (one ObsID), and remark on the non-integer frequency ratio of the QPOs present.

The frequency ratio of the majority of Group 2 QPOs indeed significantly and systematically differs from an integer when comparing multiple power spectra, see Figs 6(a) and 9.

The residuals of the best proportionality fit of $QPO_{\frac{1}{2}}$ (in *green*), QPO_2 (in *blue*), and QPO_3 (in *magenta*) with QPO_1 in Group 1 are plotted in Fig. 6(c). We find that the negative *blue* $\sim 3\sigma$ residuals around 3 Hz can be explained by the fit function not precisely matching the data. As an example of this, we plot the fit and residuals of observation 80138-01-06-00 in Fig. A18. By fitting a single Lorentzian, we appear to overestimate the centroid frequency of QPO_1.

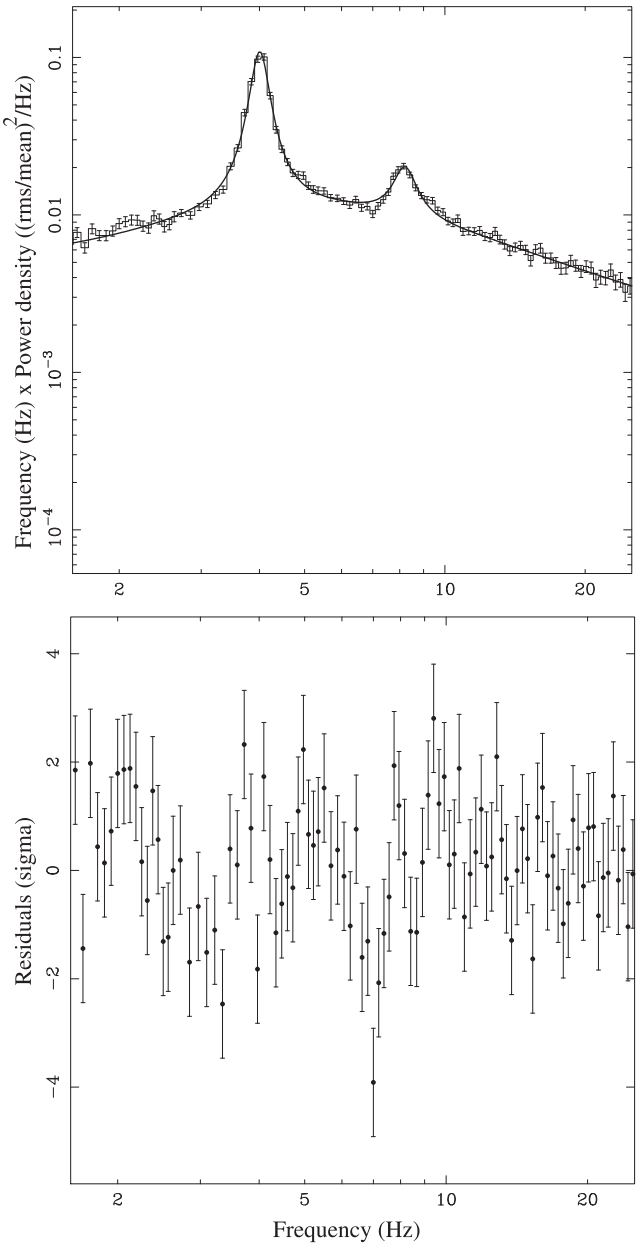

Figure A13. Fit and residuals to XTE J1550–564 observation 50134-02-01-01. We find that a Lorentzian does not perfectly describe QPO_2 with $\nu_2 = 8.19 \pm 0.03$ Hz.

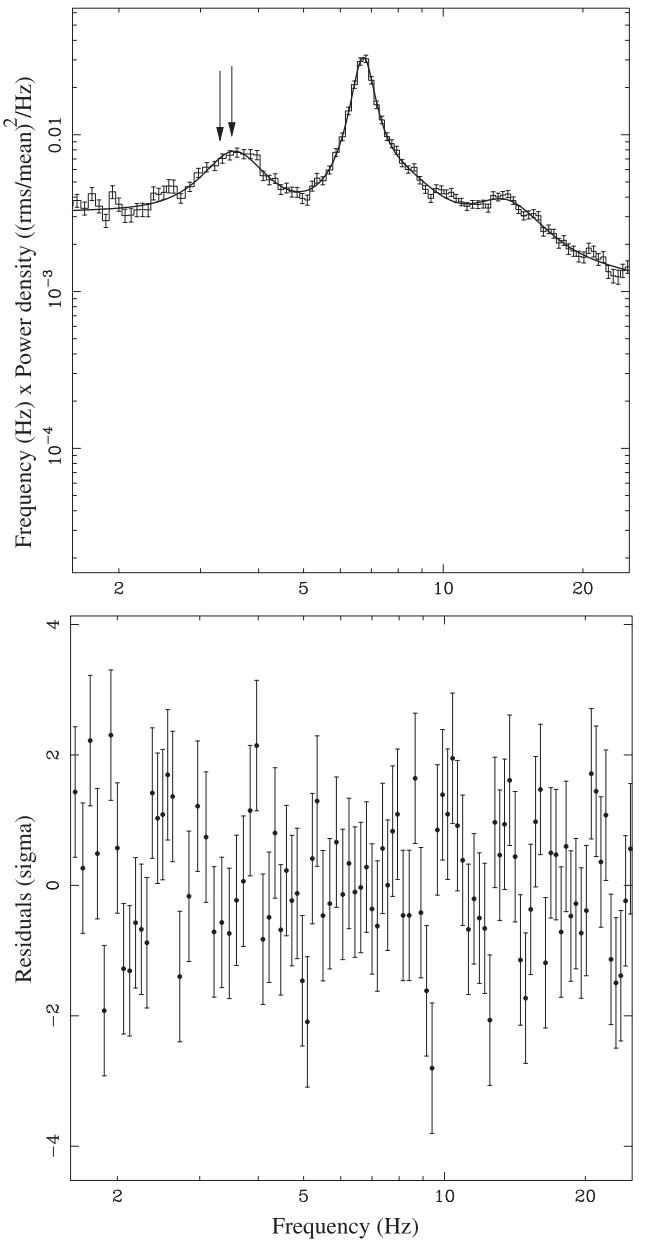

Figure A14. Fit and residuals to XTE J1550–564 observation 30191-01-31-01. The centroid frequency of the best-fitting sub-harmonic is indicated with the arrow at $\nu_{\frac{1}{2}} = 3.49 \pm 0.03$, the expected sub-harmonic centroid frequency of exactly half the fundamental frequency $\nu_{\frac{1}{2}} = 3.35$ is indicated with the leftmost arrow.

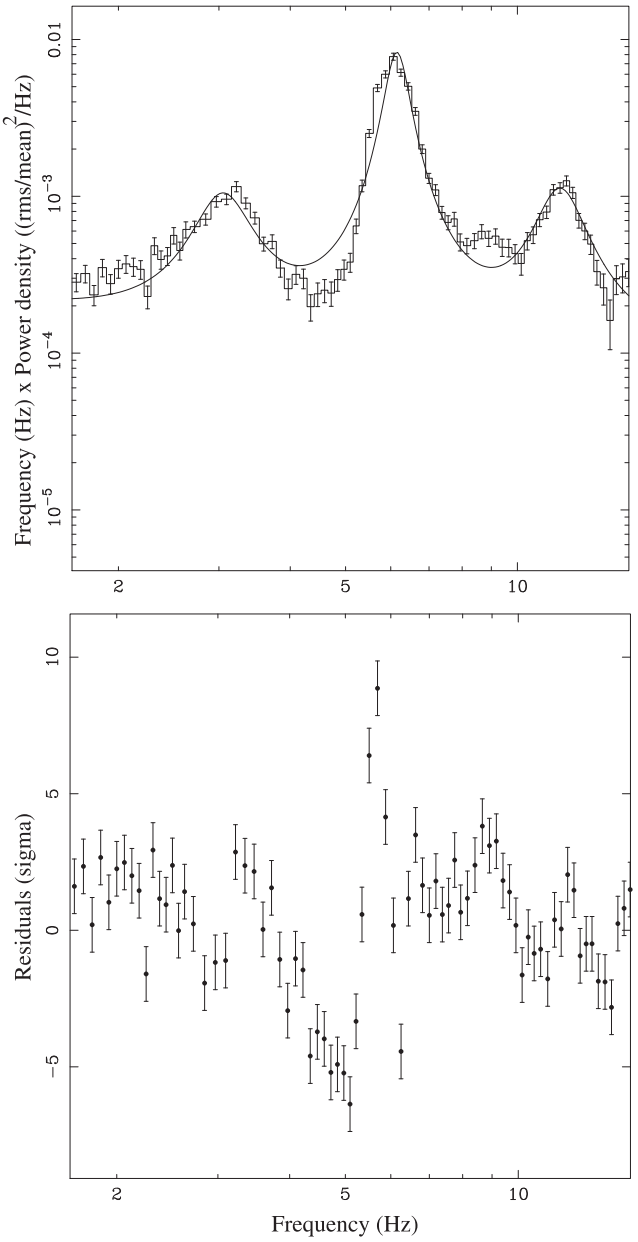

Figure A15. Fit and residuals to XTE J1550–564 observation 40401-01-55-00. A Lorentzian does not perfectly describe QPO_1 with $\nu_2 = 6.14 \pm 0.01$ Hz.

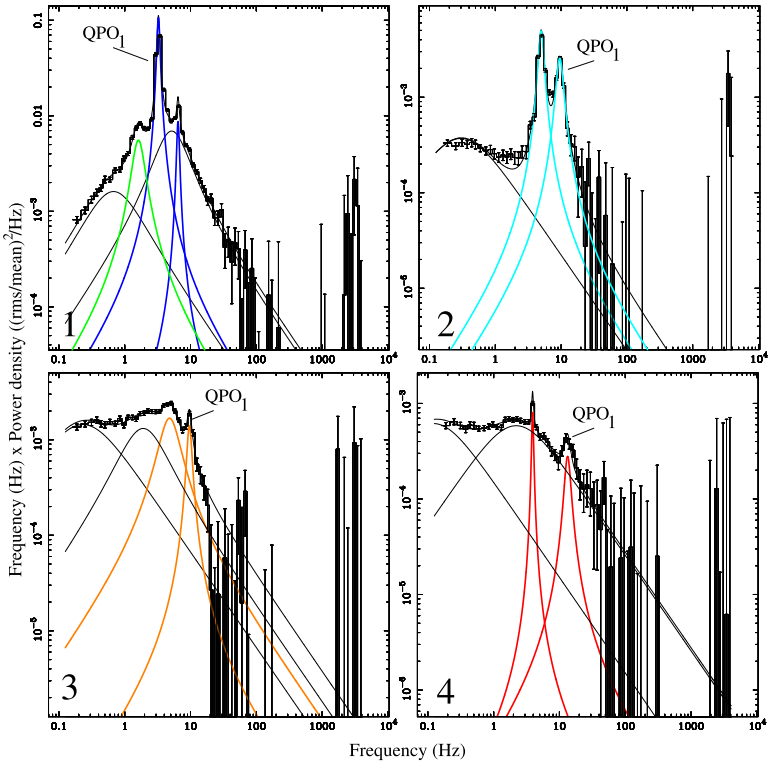

Figure A16. As in Fig. A1, but for H 1743–322. The observations used are in a clockwise direction from the top left: 80146-01-38-00, 80146-01-05-00, 80146-01-65-00, and 80146-01-07-00.

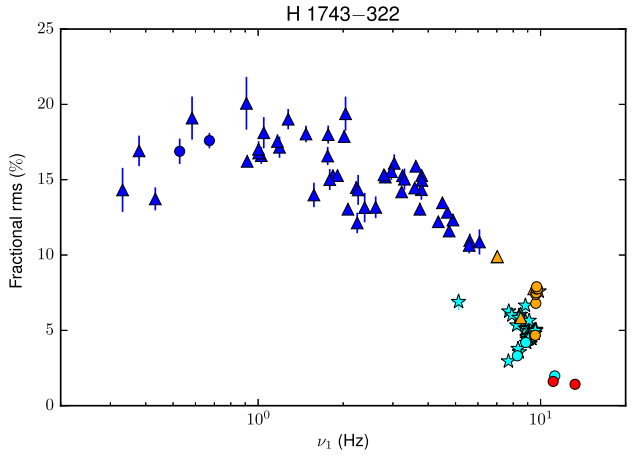

Figure A17. Fractional rms versus QPO_1 for H 1743-322. Colours and symbols correspond to those used in Fig. 6(a).

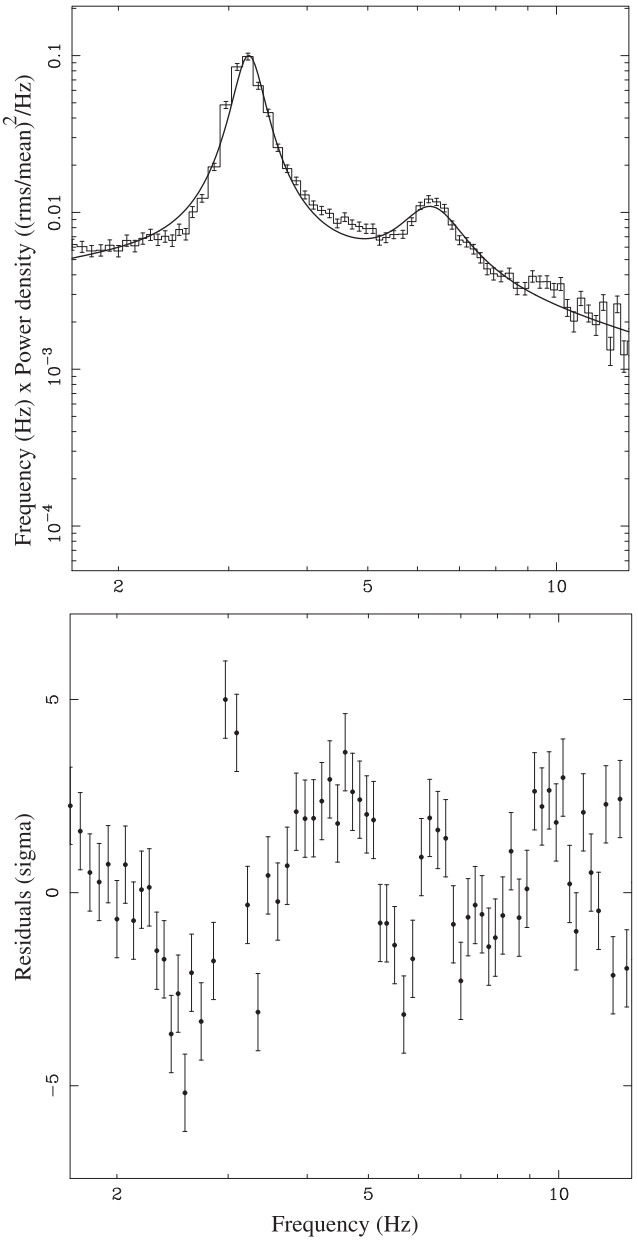

Figure A18. Fit and residuals to H 1743–322 observation 80138-01-06-00. A Lorentzian does not perfectly describe QPO_1 with $\nu_2 = 3.22 \pm 0.005$ Hz.

This paper has been typeset from a TEX/LATEX file prepared by the author.